PHILOSOPHICAL TRANSACTIONS OF THE ROYAL SOCIETY A MATHEMATICAL, PHYSICAL & ENGINEERING SCIENCES

Reactions with radioactive beams and explosive nucleosynthesis

M. Wiescher, H. Schatz and A. E. Champagne

Phil. Trans. R. Soc. Lond. A 1998 **356**, 2105-2136
doi: 10.1098/rsta.1998.0265

THE ROYAL SOCIETY

Reactions with radioactive beams and explosive nucleosynthesis

By M. Wiescher[1], H. Schatz[1] and A. E. Champagne[2]

[1]*Department of Physics, University of Notre Dame, Notre Dame, IN 46556, USA*
[2]*Department of Physics, University of North Carolina, Chapel Hill, USA and Triangle Universities Nuclear Laboratory, Duke University, Durham, USA*

This paper summarizes our present understanding of nuclear reactions with short-lived particles, which are relevant for the nucleosynthesis and energy generation in explosive stellar scenarios. It discusses the need for data on reactions far off stability and presents a short description of the present possibilities for measurements with radioactive beams. The paper presents an overview of the nucleosynthesis aspects for different explosive burning scenarios. The possible influence of proton capture reactions on short-lived nuclei are discussed for explosive hydrogen burning in novae and X-ray bursts. Also discussed are various aspects of weak-interaction processes during the collapse phase of a type-II supernova. Finally, we present key reactions for the onset of the α recombination in the neutrino-driven shock of type-II supernovae, and discuss nuclear structure effects for the r-process path.

Keywords: nucleosynthesis; supernovae; r-process; radioactive beam; luminosity

1. Introduction

One of the great successes of nuclear astrophysics has been its interpretation of the observed galactic isotopic abundance distribution in terms of primordial and stellar nucleosynthesis processes (Burbidge *et al*. 1957; Wagoner 1973; Fowler 1984). By probing the electromagnetic spectrum from infrared to γ-ray wavelengths, space-based observatories have multiplied the amount of information about abundance distributions in the winds of massive stars, in the ejecta of nova and supernova, and about galactic γ-ray sources. This in turn links the production of various elements directly with certain sites. At the same time, advances in computing allow the development of increasingly sophisticated models of stellar hydrodynamics that, in explosive events, are driven by the nuclear processes. A complete interpretation of the observed energy generation and the ejected elemental and isotopic abundances (Anders & Grevesse 1989) requires a detailed understanding of the underlying nuclear physics.

Both nucleosynthesis and energy generation depend upon the time-scales of the relevant nuclear processes. While exceedingly slow throughout most of a star's life, they become exceedingly fast in explosive conditions, leading to the dramatic increase in the brightness of novae and supernovae (Truran 1982; Arnett 1996). Quiescent nuclear burning is characterized by processes such as the pp-chains, the CNO-cycles, the He- and C-burning sequences (Rolfs & Rodney 1988; Rolfs & Barnes 1990) and the s-process (Käppeler *et al*. 1989) that occur with time-scales much longer than a typical nuclear β-decay lifetime. On the other hand, reactions taking place in an

explosive environment, where extremes of temperature and density are encountered, are often much faster than the time-scales for β-decay. Under such conditions, nuclear reactions can occur far from β-stability. Therefore, an understanding of them requires detailed studies of nuclear structure, nuclear reactions, and decay mechanisms for unstable nuclei. Current models applied to these scenarios are often based on rather crude predictions for nuclear reaction rates and decay properties. While the basic concept of nucleosynthesis and energy generation in explosive stellar processes is well understood, detailed experimental information combined with improved observational data will often allow a much deeper analysis of the hydrodynamic conditions of dynamic events such as novae, X-ray bursts and supernovae.

The study of the nuclear physics of hot or explosive stellar environments is one of the frontier issues facing nuclear astrophysics. Much of the required information can be obtained from measurements involving radioactive ion beams or radioactive targets. Because explosive nucleosynthesis occurs at high temperatures, the energies of interest are higher, and the effective range of stellar energies (Gamow window) is broader than those associated with quiescent stellar burning (Rolfs & Rodney 1988; Rolfs & Barnes 1990). Therefore, cross-sections for proton- and α-capture reactions are higher than those usually encountered in nuclear astrophysics. Nonetheless, these reactions are still extremely difficult to study, owing to the low beam intensities and conditions of high background radiation that typify current radioactive-beam measurements. To meet this challenge, a number of radioactive-beam facilities have been constructed and more are planned for the near future. In the following, we will describe some of the reaction processes of explosive nucleosynthesis and summarize some of what has been learned about them. In so doing, we will highlight the successes and problems associated with experiments using radioactive beams. We will also try to identify areas where more nuclear data are needed and their expected influence on our understanding of nucleosynthesis and energy generation.

2. Nuclear physics input

(a) *Reaction networks*

In general, energy generation and nucleosynthesis in stellar burning can be simulated by solving large-scale nuclear-reaction networks for the temperature and density conditions of interest. Such a calculation follows the time evolution of the isotopic abundances $Y_i = X_i/A_i$ (mass fraction divided by mass number) as a function of temperature and density, and determines the reaction flux through the nuclei in the network. The latter defines the actual reaction path taken for a particular temperature and density. Of course, temperature and density are dynamic quantities. Therefore, it is important to compare and correlate the macroscopic time-scale with the nuclear time-scale within the framework of a stellar model.

A reaction network is defined as a set of differential equations describing the various isotopic abundances as a function of time. The time derivative of the abundance of each isotope is expressed in terms of the reaction rates of the different production and depletion reactions,

$$\frac{\mathrm{d}Y_i}{\mathrm{d}t} = \sum_j N_j^i \lambda_j Y_j + \sum_{j,k} N_{j,k}^i \rho N_\mathrm{A} \langle j,k \rangle Y_j Y_k + \sum_{j,k,l} N_{j,k,l}^i \rho^2 N_\mathrm{A}^2 \langle j,k,l \rangle Y_j Y_k Y_l, \quad (2.1)$$

where λ_j denotes various decay processes (including photodisintegration), $\rho N_{\rm A}\langle j,k\rangle$ refers to two-particle reactions, and $\rho^2 N_{\rm A}^2\langle j,k,l\rangle$ accounts for three-particle interactions. The quantity ρ is the density of the gas and $N_{\rm A}$ represents Avogadro's number. The individual N^i may be written as $N^i_j = N_i$, $N^i_{j,k} = N_i/(N_j!N_k!)$, and $N^i_{j,k,l} = N_i/(N_j!N_k!N_l!)$. The N_i may be positive or negative and specify how many particles of species i are created or destroyed in the reaction. The factors appearing in the denominators are introduced in order to avoid double-counting for cases involving reactions of identical particles. For a more detailed discussion, see Fowler *et al.* (1967, 1975). At the extreme conditions encountered in supernovae, a typical interaction time can be much shorter than a typical dynamical time for the system. In this circumstance, the individual abundances will approach an equilibrium (i.e. $\mathrm{d}Y_i/\mathrm{d}t = 0$), which leads to some simplification in the solution of equation (2.1). For example, the rapid neutron-capture process (r-process) can be modelled by using conditions appropriate for sustaining a β-flow equilibrium as well as an (n,γ)–(γ,n) equilibrium (as will be discussed below). The latter condition implies that neutron-capture cross-sections are less important than the neutron separation energies that regulate the equilibrium abundances.

The time-integrated net reaction flow between two isotopes i and j is defined by

$$F_{i,j} = \int \left[\frac{\mathrm{d}Y_i}{\mathrm{d}t}_{(i\to j)} - \frac{\mathrm{d}Y_j}{\mathrm{d}t}_{(j\to i)} \right] \mathrm{d}t. \tag{2.2}$$

The maximum flux $F_{i,j}$ defines the main reaction path along which nucleosynthesis will take place. As an example, figure 1 shows the main reaction path for hydrogen burning at temperatures $T = 4\times10^8$ K and densities of $\rho = 10^4$ g cm^{-3}, integrated over a processing time of 1000 s. The main flow is characterized by a sequence of proton captures (hydrogen burning) and β-decays at the neutron-deficient side of the line of stability. This process, of importance in explosive, hydrogen-rich environments has been named the rapid proton-capture (rp)-process (Wallace & Woosley 1981) and will be discussed in more detail below.

The observed luminosity of a star is simply equal to the power generated in its interior. The energy production ϵ by nuclear processes can be determined from the net-reaction flow and the corresponding Q-values $Q_{i,j}$ for the contributing reactions,

$$\epsilon = \sum_{i,j} F_{i,j} Q_{i,j}. \tag{2.3}$$

The time evolution of the isotopes, the time-integrated reaction flux, and the energy production rate depend critically on the pertinent thermonuclear reaction rates involved in a given process. An accurate knowledge of these rates is therefore essential for a reliable interpretation of the nucleosynthesis.

(*b*) *Reaction rates*

As discussed above, complete network calculations include rates for all relevant decay processes, photodisintegration, and two- or three-body interactions. However, in the following we will restrict our consideration to β-decay and two-particle interactions. A detailed discussion of the rates for photodisintegration and three-particle interactions is beyond the scope of this paper, but can be found in the literature (Fowler *et al.* 1967, 1975; Cowan *et al.* 1991; Görres *et al.* 1995*a*; Schatz *et al.* 1997*a*).

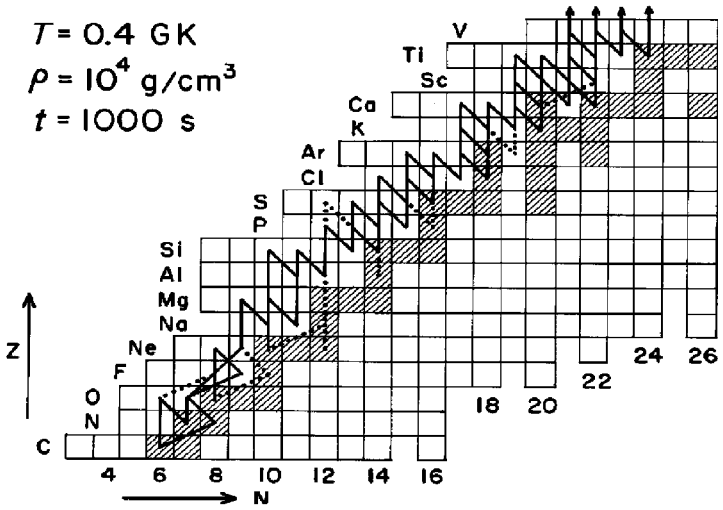

Figure 1. Reaction path in hot hydrogen burning at a temperature of 0.4 GK and a density of 10^4 g cm^{-3}. The total flux has been integrated over $t = 1000$ s. The dotted lines indicate a weak flux of less than 1%.

The decay rate for a β-unstable nucleus i, λ_i can be determined from the measured lifetime τ_i or half-life $T_{1/2}$,

$$\lambda_i = \frac{1}{\tau_i} = \frac{\ln 2}{T_{1/2}}. \tag{2.4}$$

If the half-life has not been measured, then the decay rate can be calculated from the β-strength function $S_\beta(E)$ via

$$\lambda_i = \frac{g_v^2 m_e^5 c^4}{2\pi^3 \hbar^7} \int_0^{Q_\beta} S_\beta(E) f_0(Z, Q_\beta - E)\, \mathrm{d}E. \tag{2.5}$$

In this equation g_v represents the vector coupling constant, and $f_0(Z, Q_\beta - E)$ is the Fermi function. The β-strength function,

$$S_\beta(E) = \sum_{J,\pi} B(E, J, \pi)\rho(E, J, \pi), \tag{2.6}$$

describes the energy dependence of the transition probability and is expressed in terms of a reduced transition probability $B(E_i, J, \pi)$ to a final state at excitation energy E_i with spin-parity J^π, weighted by the level density for spin and parity J^π (Fuller *et al.* 1980). The reduced transition probability must either be calculated or deduced from experimental information (as described below). For scenarios such as the r-process (Kratz *et al.* 1993) or the rp-process (Schatz *et al.* 1997*a*), reactions occur at a rapid pace and consequently the reaction paths run far from stability. Hence, the time-scale for nucleosynthesis and the rate of energy generation are determined by the lifetimes for the various β-decays encountered along the reaction path. Therefore, extending the experimental database requires the production of short-lived nuclei (e.g. by heavy-ion fragmentation). However, it is not sufficient to measure the decay of a nucleus in its ground state if it will be thermally excited in the stellar medium. It is technically feasible to measure decays from isomeric levels by first preparing them as a beam and then storing them, but this technique is

limited to rather long-lived levels. For short-lived excited states, we presently rely on theoretical predictions.

The stellar reaction rate for a two-particle interaction, $N_{\mathrm{A}}\langle\sigma v\rangle$ is determined by a folding of the reaction cross-section $\sigma(E)$ with the Maxwell–Boltzmann energy distribution of the interacting particles. The reaction rate can be expressed as a function of temperature by

$$N_{\mathrm{A}}\langle\sigma v\rangle = \left(\frac{8}{\pi\mu}\right)^{1/2}(kT)^{-3/2}\int\sigma(E)E\mathrm{e}^{(-E/kT)}\,\mathrm{d}E, \tag{2.7}$$

where μ is the reduced mass and E is the interaction energy (in the centre of mass). Because stellar energies are well below the Coulomb barrier, the cross-section for a non-resonant reaction decreases exponentially with decreasing energy. For resonant reactions that produce compound nuclei with a high level density (e.g. for the case high Q-value reactions and/or heavy targets) the cross-section can be approximated by Hauser–Feshbach calculations (Rauscher *et al*. 1997). In cases involving a low density of final states (for example, near closed-shell nuclei or close to the drip-lines), the cross-section is determined by isolated resonances and can be described by the usual Breit–Wigner form. In these cases, the reaction rate is expressed in terms of the resonance energy E_{r} and the resonance strength, $\omega\gamma$,

$$N_{\mathrm{A}}\langle\sigma v\rangle = N_{\mathrm{A}}\left(\frac{2\pi}{\mu kT}\right)^{3/2}\hbar^2\omega\gamma\mathrm{e}^{-E_{\mathrm{r}}/kT}. \tag{2.8}$$

The resonance strength is a function of the partial widths for the entrance and exit channels, Γ_{in}, Γ_{ex}, respectively, and the total resonance width Γ_{tot},

$$\omega\gamma = \frac{2J+1}{(2j_{\mathrm{p}}+1)(2j_{\mathrm{t}}+1)}\frac{\Gamma_{\mathrm{in}}\Gamma_{\mathrm{ex}}}{\Gamma_{\mathrm{tot}}}. \tag{2.9}$$

Here, J, j_{p}, j_{t} are the spins of the resonance state, the projectile, and the target, respectively. In order to specify the stellar reaction rate, the cross-sections for the resonant and non-resonant reaction contributions have to be known in the stellar energy range.

(*c*) *Experimental approach*

To understand the nucleosynthesis of stellar explosions, it is necessary to study reactions involving radioactive nuclei. Radioactive targets can be used for cross-section measurements, but they are restricted to nuclei having fairly long half-lives, e.g. for ^{7}Be, ^{22}Na, ^{26}Al, or ^{44}Ti. Shorter half-lives require the use of radioactive beams.

Capture measurements with radioactive beams in inverse kinematics are among the major goals for radioactive-beam facilities. Previous measurements at first-generation facilities were handicapped by shortcomings in the detection systems employed, which lead to low efficiencies and high background levels. These conditions can be improved considerably by the use of high-granularity detector clusters (where the granularity is used to minimize the background rate in any one detector) coupled to a high-resolution recoil mass separator (with a rejection of the primary beam on the order of less than 10^{-13}). Further background reduction can be achieved by imposing coincidence requirements or by careful particle identification. As in the case

of measurements using high-intensity stable beams, stoichiometry and resiliency of the target are important considerations for radioactive-beam measurements. Solid-compound targets such as CH_2, while easy to fabricate, will degrade with time, which imposes a systematic correction on the experimental results (Galster *et al.* 1991). In addition, the number of active target nuclei in some energy interval will necessarily be lower than would be the case for a pure target. However, a pure H_2 or He target for low energy reactions requires a windowless gas target system. Gas targets with desirable specifications can be constructed either as gas-cell (Rolfs *et al.* 1978; Bittner *et al.* 1979) or as gas-jet (Becker *et al.* 1982; Görres *et al.* 1985). The gas cell represents an extended target and therefore its use requires additional corrections for cross-section measurements. Its main advantage is that high target densities and favourable stoichiometry can be obtained rather easily (Görres *et al.* 1980). A gas-jet system in principle maintains the advantages of a quasi-point-source. For these conditions, however, only a limited target density of *ca.* 10^{18} parts per cm^2 can be achieved with light target gases like hydrogen and helium. Caution is always required for the determination of absolute cross-sections because of possible reaction contributions from the extended jet halo. The necessary corrections depend critically on the respective jet design (Hilgemeier *et al.* 1988).

For measurements of decays, masses or half-lives, the radioactive beam itself is the subject of study. Suitable beams can be produced via projectile fragmentation using a high-quality fragment mass separator (see, for example, Mohar *et al.* 1991; Blank *et al.* 1995). Since these studies often involve heavy nuclei, the experimental focus is on accurate identification of incident mass and charge. These nuclear-structure measurements are extremely important for determining the reaction path of the r- and rp-process and the time-scales for the associated explosive events (Cowan *et al.* 1991; Schatz *et al.* 1997*a*).

Coulomb dissociation is, in principle, a powerful tool. This was beautifully demonstrated by the complementary measurements with a ^{13}N beam in inverse kinematics (Decrock *et al.* 1991) of the resonance strength in $^{13}N(p,\gamma)^{14}O$, and Coulomb dissociation of an ^{14}O beam (Motobayashi *et al.* 1991; Kiener *et al.* 1993). This is, however, an 'ideal' example because of the 100% ground state E1-transition to (and from) the resonance level. Interpretation of a Coulomb-excitation measurement is made considerably more difficult (or even impossible) if the resonance state of interest decays via a γ-cascade or with mixed multipolarities to the ground state. In this case, a reliable analysis requires an independent measurement of the decay branching and mixing. Another challenge for Coulomb dissociation arises when the reaction of interest proceeds via direct capture, such as in the case of $^{8}B(\gamma,p)^{7}Be$ (Iwasa *et al.* 1996). A reliable result requires a full understanding of possible post-acceleration effects. However, the main handicap of this method at present is the broad momentum spread of the beam, which leads to poor energy resolution. This, coupled with limits in detector resolution, restricts the applicability of this technique primarily to the analysis of single, well-separated resonance states, as was the case for $^{14}O(\gamma,p)^{13}N$.

(*d*) *Differences between laboratory and stellar rates*

Nuclei in a star are immersed in a hot bath of photons, and in principle they can be excited by photoabsorption. Therefore, reactions may involve not only the ground-

state case studied in the laboratory, but also excited states. Direct measurements of reactions for excited nuclei are virtually impossible unless the excited state is isomeric. Therefore, one is forced to rely upon available nuclear-structure information in order to calculate the rate. On the basis of temperature alone, one would guess that the effects of photoexcitation would be most problematic in supernovae. However, if conditions of quasi-equilibrium pertain, then individual reaction rates are less important (Woosley & Hoffman 1992). Fortunately, the cases involving reactions on excited states are relatively few and are found primarily in situations where reactions fall out of equilibrium, or in an extended rp-process.

High temperatures and densities could also have an influence on weak-interaction rates. If a β-unstable nucleus is excited via absorption of a photon, then the β-decay Q-value, Q_β will be increased by an amount corresponding to the excitation energy. On the basis of energetics alone, this would lead to an increase in the decay rate (Cosner & Truran 1981). In addition, if the excitation opens up more or different decay channels, then one would also expect an increase in the rate. For example, if the decay of the ground state is forbidden, but transitions from excited states are allowed, then the rate would be increased by a large factor (Cameron 1959). A dramatic illustration of this process is the case of ^{26}Al where the ground state decays to ^{26}Mg with a half-life of $T_{1/2} = 7.2 \times 10^5$ years, but where $T_{1/2}$ for the first-excited state (at $E_x = 228$ keV) is only 6.3 s. If these two states reach thermal equilibrium, then at a temperature of 10^9 K the *stellar* half-life is only 24 min.

Ionization has a very obvious effect on electron capture. If inner-shell electrons are removed from an atom, the electron-capture rate is necessarily decreased. However, ionization also affects $\beta^\pm$ decay by modifying the wave functions for the outgoing $e^\pm$ and by changing Q_β. Screening of the nuclear Coulomb potential by atomic electrons produces a slight enhancement in the β^- decay probability and a slight reduction for β^+-decay. Ionization reduces the efficiency of screening, but does not eliminate it because the continuum electrons also produce a screening potential. The net result is a rather small change in the decay rate (Bahcall 1962). On the other hand, changes in Q_β can have important consequences. Ionization simply removes electron-binding energy from the energy balance in β-decay. Since the binding energy increases with increasing nuclear charge, removing electrons lowers (raises) Q_β for β^- (β^+)-decay. For example, in Fe–Co, the Q-values for fully stripped ions and neutral atoms differ by 3.2 keV. For Pt–Au, this difference is 16 keV. Clearly, the effects of ionization are most important for heavy nuclei. Notice that in cases where the laboratory Q_β is small (less than 20 keV), β^- decay to the continuum might be completely suppressed by this reduction in Q_β. Thus, for continuum decays, ionization has the effect of lowering the β^- rate and increasing the β^+ rate. However, with a large number of empty atomic orbitals available, it is possible for β^--decay to produce an electron in a final bound state rather than in a continuum state and thereby gain the binding energy of the created electron. This bound-state β^--decay has been observed for fully stripped ^{163}Dy (Jung *et al.* 1993), a nucleus that is stable when part of a neutral atom. The added energy and phase space for bound-state decay could greatly increase the decay rate for a nucleus that is already unstable and could cause a nucleus that is stable in the laboratory to decay.

Continuum decay is also suppressed when the electron density becomes high enough to reach degeneracy. If the Fermi energy of the electron gas exceeds the decay energy, there will be no allowed final states for the decay to populate. Once

this happens, endoergic electron capture becomes energetically favourable. Electron capture in stellar environments has been treated in detail by Bahcall (1964).

Because there may be significant differences between laboratory rates and those in a stellar medium, it is important to gather enough nuclear-structure information (e.g. masses, level schemes, etc.) to make meaningful corrections when needed. Unfortunately, this information is often incomplete and most nucleosynthesis calculations employ laboratory rates. This situation will certainly improve as nuclei far from stability are studied in greater detail.

3. Explosive nucleosynthesis in novae

Novae have been interpreted as thermonuclear runaways on the surface of an accreting white dwarf within a close binary-star system (Truran 1982, 1990; Starrfield 1989). The binary system is characterized by an extended near-main-sequence star which has filled its Roche Lobe, coupled to a degenerate white-dwarf that accretes the mass lost by its companion. The dwarf can be either a carbon–oxygen (CO) white dwarf which has formed after the He-burning stage of its evolution, or an oxygen–neon–magnesium (ONeMg) white dwarf which has developed after the carbon burning stage (Law & Ritter 1983). The accreted material forms a thin, but highly dense envelope at the surface of the white dwarf. Dredge-up of the underlying white-dwarf material (^{4}He, ^{12}C, ^{16}O in the case of an CO-white dwarf; ^{16}O, ^{20}Ne, and ^{24}Mg in the case of an ONeMg-white dwarf) leads to an enrichment of heavier isotopes within the envelope (Glasner *et al.* 1997). After a 'critical' mass has been accreted, thermonuclear ignition takes place at the bottom of the accreted envelope. The conditions governing the onset of burning depend sensitively on the mass of the white dwarf and on the accretion rate. If the envelope is allowed to cool sufficiently, then ignition will occur under degenerate conditions, presumably via the pp-chains, which leads to a rapid increase in temperature at constant pressure and density. This 'thermonuclear runaway' is further enhanced as the pre-existing ^{12}C and ^{16}O act as catalysts for the hot CNO cycles. Degeneracy is lifted once the local temperature exceeds the Fermi temperature T_{F} for the material, given by

$$T_{\mathrm{F}} = 3.03 \times 10^5 (\rho/\mu_{\mathrm{e}})^{2/3}, \tag{3.1}$$

where ρ is the density (in g cm^{-3}) and μ_{e} is the electron mean molecular mass (Starrfield 1989; Hansen & Kawaler 1994). Because the temperature in the burning shell rises rapidly, the peak temperature can exceed the Fermi temperature before the electron gas is sufficiently non-degenerate to initiate expansion. This allows a convective zone to develop at the base of the envelope which gradually grows to the surface as the temperature continues to increase. Energy is thereby transported to the surface quite rapidly, i.e. within the convective time-scale of $t_{\mathrm{conv}} \approx 10^2$ s. Within this short time period, an appreciable fraction of the long-lived β^+ emitters that are produced by the hot CNO cycles are carried to the surface. The release of decay energy further increases the luminosity to a level in excess of $10^5 L_\odot$. This super-Eddington luminosity, produced on the short convective time-scale, causes rapid expansion and ejection of the envelope (Shore *et al.* 1994).

Typical nova outbursts occur with densities of approximately $\rho \approx 10^3$ g cm^{-3} and typical peak temperatures between 1×10^8 and 4×10^8 K (Starrfield 1989; Starrfield *et al.* 1998). For illustration, figure 2 shows a temperature profile for the hydrogen-burning zone at the bottom of the envelope as calculated for a classical nova involving

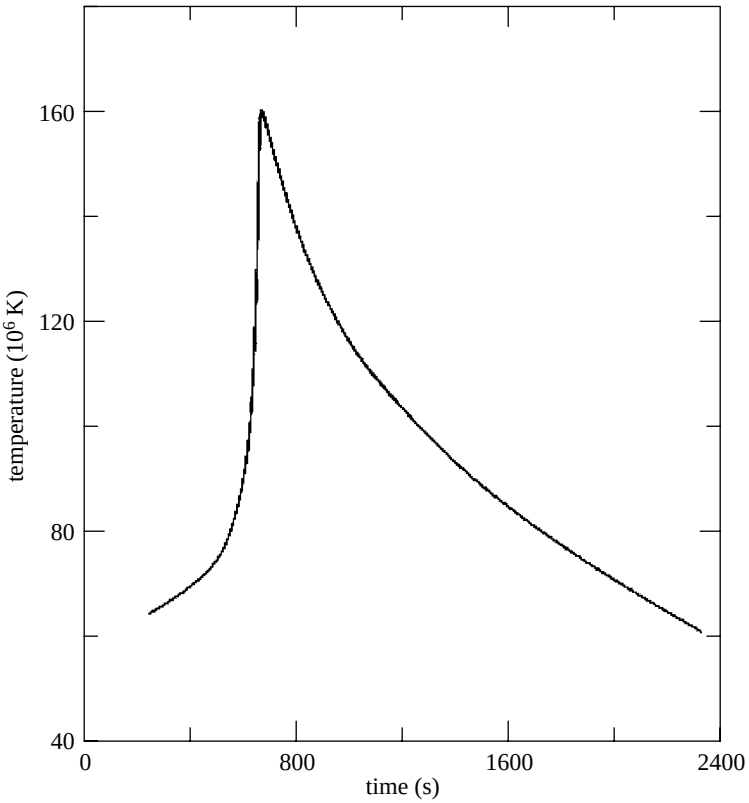

Figure 2. Temperature profile during the thermonuclear runaway of a classical nova.

a $1.0M_{\odot}$ CO-white dwarf (Starrfield 1989). For comparison, figure 3 shows the temperature profile for a thermonuclear runaway on the surface of a $1.25M_{\odot}$ ONeMg white dwarf (Starrfield *et al*. 1998).

Because the ejecta of these novae are enriched in Ne compared to the solar Ne abundance they are called Ne-novae. The figures indicate that the thermonuclear runaway on the surface of an ONeMg white dwarf can produce considerably higher peak temperatures than is the case for a CO white dwarf. This has implications for nucleosynthesis, as will be discussed below.

Nucleosynthesis in a classical nova occurs primarily as a consequence of the hot CNO cycles (Glasner *et al*. 1997). Figure 4 shows the main reaction flow integrated over the duration of the outburst shown in figure 2. The calculation has been performed by assuming solar initial abundances with enrichments of ^{12}C and ^{16}O. The initial ^{12}C is converted to ^{14}O by two sequential proton capture reactions, $^{12}\mathrm{C}(\mathrm{p},\gamma)^{13}\mathrm{N}(\mathrm{p},\gamma)^{14}\mathrm{O}$. A measurement of the strong resonance in $^{13}\mathrm{N}(\mathrm{p},\gamma)^{14}\mathrm{O}$ has been subject of the first successful radioactive-beam experiment at Louvain-la-Neuve (Decrock *et al*. 1991). However, some uncertainties still remain in the magnitude of the non-resonant direct-capture component of the reaction rate. The decay of ^{14}O to ^{14}N allows the reaction flow to proceed to ^{15}O by $^{14}\mathrm{N}(\mathrm{p},\gamma)$. Because of their slow β-decay rates, both, ^{14}O ($T_{1/2} = 70.59$ s) and ^{15}O ($T_{1/2} = 122.24$ s) become enriched. A second CNO cycle is triggered by the $^{16}\mathrm{O}(\mathrm{p},\gamma)^{17}\mathrm{F}$ reaction, which is dominated

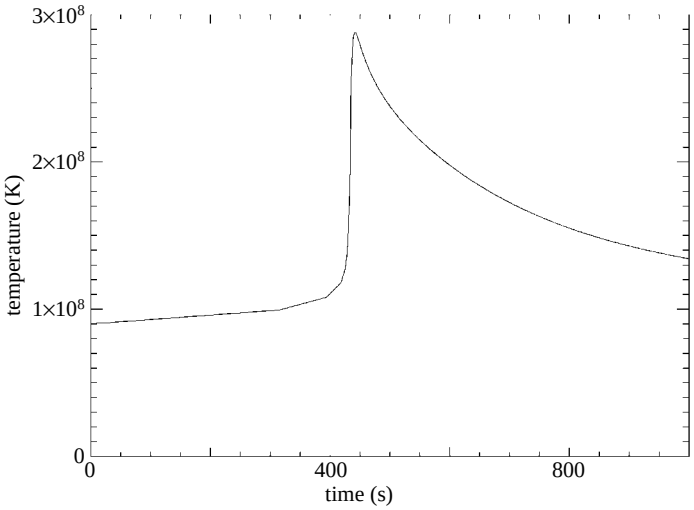

Figure 3. Temperature profile during the thermonuclear runaway of a Ne-nova.

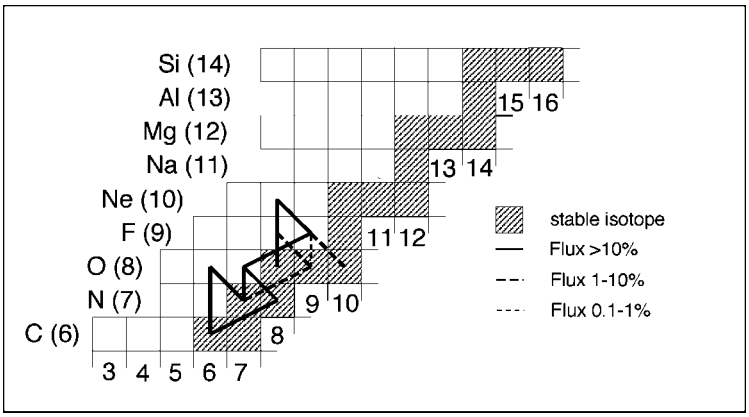

Figure 4. Reaction flux during explosive hydrogen burning in classical CO-nova. The net flow is integrated over the period of the explosion.

by direct capture (Rolfs 1973). The fate of the ^{17}F depends on the reaction rate for $^{17}\mathrm{F}(\mathrm{p},\gamma)^{18}\mathrm{Ne}$ which has not been measured yet. Several estimates for this rate have been reported (Wiescher *et al*. 1988*a*; Garcia *et al*. 1991; Hahn *et al*. 1996) and are based on experimental and theoretical studies of the level structure in the compound nucleus ^{18}Ne. The results indicate that the (p,γ) reaction dominates β-decay for temperatures above $T = 2 \times 10^8$ K, higher than the peak temperature in classical novae. The reaction sequence $^{17}\mathrm{F}(\beta^+\nu)^{17}\mathrm{O}(\mathrm{p},\alpha)^{14}\mathrm{N}$ processes the material into the first CNO cycle causing further enrichment of ^{15}O by $^{14}\mathrm{N}(\mathrm{p},\gamma)^{15}\mathrm{O}$. A distinguishing feature in the abundance distribution of the ejecta is a large overabundance of nitrogen (Williams 1982) originating from the decay of ^{14}O, and ^{15}O that has been transported out of the burning zone and into the envelope.

A large number of novae also show enhancements in neon (Truran & Livio 1986; Weiss & Truran 1990; Livio & Truran 1994) as compared to the solar abundance (Anders & Grevesse 1989). This has been interpreted as originating from a ther-

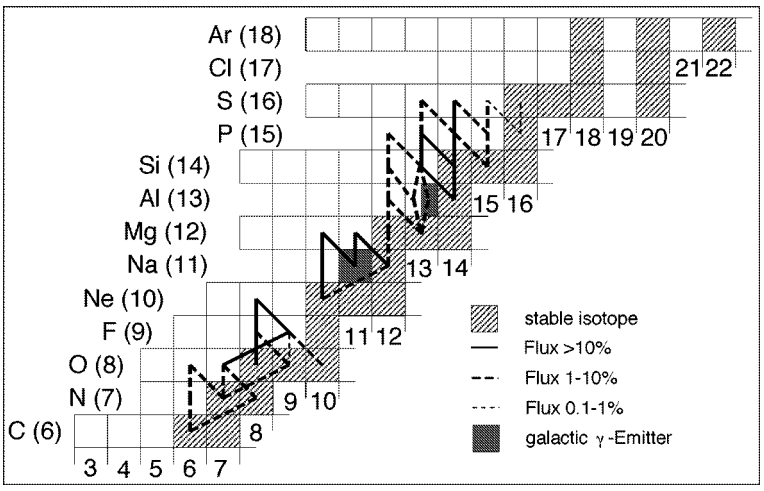

Figure 5. Reaction flux during explosive hydrogen burning in Ne-novae. The net flow is integrated over the duration of the outburst.

monuclear runaway on the surface of an accreting ONeMg white dwarf (Weiss & Truran 1990). Additional observation of elements up to sulphur are taken as evidence of the high temperatures that would lead to an rp-process (Politano *et al.* 1995; Coc *et al.* 1995; Jose *et al.* 1997; Starrfield *et al.* 1998). Figure 5 shows the reaction flux for a Ne-nova, calculated for the hydrogen-burning zone at the base of the accreted layer. Since ^{16}O is dredged up from the upper layers of the white dwarf, the hot CNO cycles also contribute to the nucleosynthesis but to a smaller extent than in classical novae. The nucleosynthesis of ^{16}O, ^{18}Ne, ^{18}F, and ^{15}O is shown in figure 6. Because of the higher peak temperatures predicted for Ne-novae (see figure 3), ^{17}F is depleted by proton capture rather than by β-decay. Consequently, as the temperature rises, the initial abundance of ^{16}O is rapidly depleted and converted, via $^{16}\mathrm{O}(\mathrm{p},\gamma)^{17}\mathrm{F}(\mathrm{p},\gamma)^{18}\mathrm{Ne}$, into ^{18}Ne which has a rather long lifetime of $\tau_\beta(^{18}\mathrm{Ne}) = 2.41$ s. The β-decay of ^{18}Ne leads to the production of ^{15}O via $^{18}\mathrm{Ne}(\beta^+\nu)^{18}\mathrm{F}(\mathrm{p},\alpha)^{15}\mathrm{O}$. Since ^{15}O is fairly long-lived, ($T_{1/2} = 122.24$ s), it survives until the expansion phase where it is rapidly mixed to the surface of the envelope. The ejected outer shell therefore contains a large amount of freshly produced ^{15}N. Note that this picture does not lead to a sizeable inventory of ^{18}F. This point is significant because if a quantity of ^{18}F survives to the expansion phase, then the annihilation photons produced as a consequence of its β^+ decay ($T_{1/2} = 109.8$ min) could be detectable (Leising & Clayton 1987). However, a detailed, quantitative description of these processes requires an exact knowledge of the relevant reaction rates. These include the reactions involving the radioactive fluorine isotopes, ^{17}F and ^{18}F. An experimental verification of the predicted reaction rates requires detailed measurements of the cross-sections for the various resonant and non-resonant reaction contributions. Because both ^{17}F and ^{18}F are rather short-lived, these experiments can only be performed by producing radioactive fluorine beams. While several measurements to determine the reaction rate of $^{18}\mathrm{F}(\mathrm{p},\alpha)^{15}\mathrm{O}$ at higher temperatures have been successfully completed at Louvain-la-Neuve (Coszach *et al.* 1995; Graulich *et al.* 1997) and Argonne (Rehm *et al.* 1996), a measurement of the $^{17}\mathrm{F}(\mathrm{p},\gamma)^{18}\mathrm{Ne}$ reaction is still awaited.

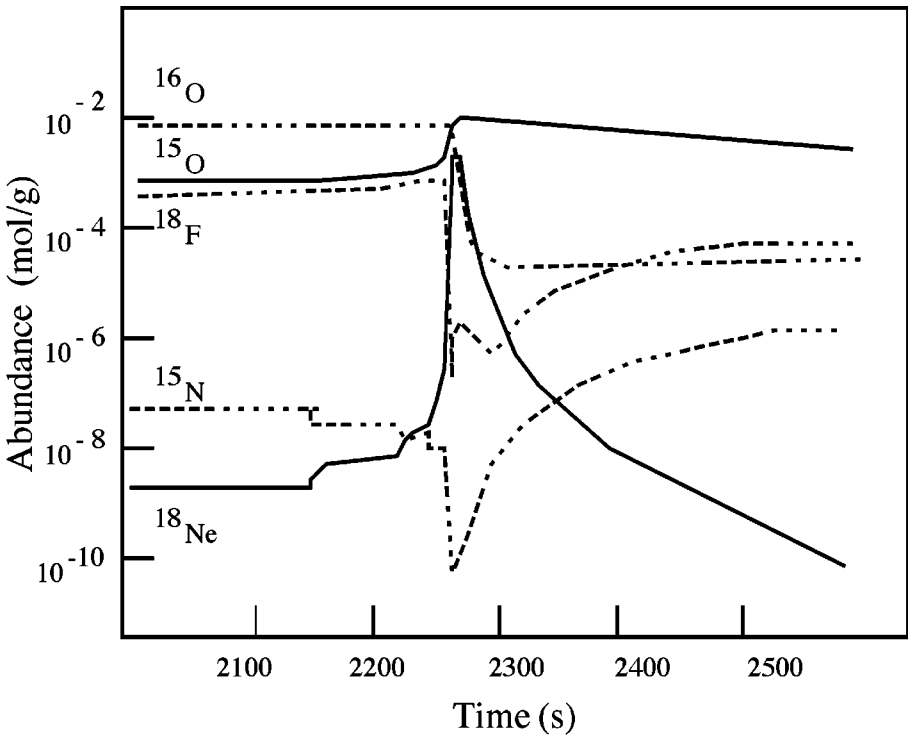

Figure 6. Nucleosynthesis in the hot CNO cycles for a Ne-nova.

Figure 5 also shows strong indications for nucleosynthesis by the NeNa- and the MgAl cycles. These reactions are triggered by the initially high ^{20}Ne and ^{24}Mg abundances in the dredged-up material. Nucleosynthesis via the NeNa- and the MgAl-cycles for novae conditions is not fully understood, owing to large uncertainties in the reaction rates for both the stable and unstable isotopes. Calculations based on the most recent data and model compilations (Caughlan & Fowler 1988; Herndl *et al*. 1995; Iliadis *et al*. 1996*a*) predict significant production of the long-lived γ-emitters ^{22}Na and ^{26}Al (Politano *et al*. 1995; Coc *et al*. 1995; Wanajo *et al*. 1997; Starrfield *et al*. 1998). A recent observation of two Ne novae, Her1991 and Cyg1992, by the COMPTEL Gamma Ray Observatory yielded only upper limits for the characteristic γ-rays from the decay of ^{22}Na (1.275 MeV) (Iyudin *et al*. 1995). This indicates a substantially lower ^{22}Na abundance in the ejecta than is predicted by model calculations (Politano *et al*. 1995; Wanayo *et al*. 1997; Starrfield *et al*. 1998). In the case of ^{26}Al it has been argued that novae can produce only a small fraction of the observed galactic distribution (Prantzos & Diehl 1995; Jose *et al*. 1997). This conclusion is based not only on nucleosynthesis considerations, but also on the morphology of the γ-ray emission observed with the COMPTEL observatory (Prantzos & Diehl 1995). However, the observations themselves do not rule out some diffuse emission from novae.

At the onset of the thermonuclear runaway, ^{22}Na is formed by the classical NeNa cycle (Marion & Fowler 1957) via $^{20}\mathrm{Ne}(\mathrm{p},\gamma)^{21}\mathrm{Na}(\beta^{+}\nu)^{21}\mathrm{Ne}(\mathrm{p},\gamma)^{22}\mathrm{Na}$. Figure 7 shows the development of the abundances in the NeNa cycle during the outburst. An equilibrium abundance of ^{22}Na is quickly established between the production and

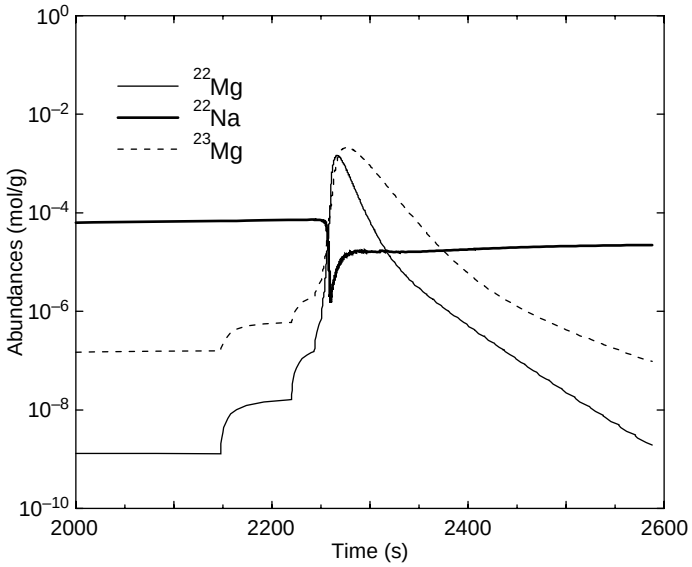

Figure 7. Nucleosynthesis in the hot NeNa cycles in Ne-nova burning. The initial amount of ^{20}Ne is converted to ^{22}Mg which subsequently decays to ^{22}Na. The ^{22}Na is then converted to ^{23}Mg by proton capture.

its depletion via the ^{22}Na(p, γ)^{23}Mg reaction which has been studied extensively in recent years (Seuthe *et al*. 1990; Schmidt *et al*. 1995; Stegmüller *et al*. 1996).

With the increase in temperature, the rate for ^{21}Na(p, γ)^{22}Mg exceeds that for the β-decay of ^{21}Na and the hot NeNa cycle emerges. The latter reaction rate is based on estimates about the level structure of the compound nucleus ^{22}Mg (Wiescher *et al*. 1986) and measurements of the excitation energies of the proton unbound states (Wiescher & Langanke 1986). A measurement of the rate with a radioactive ^{21}Na beam is needed to quantify the ^{22}Na production in the initial phase of the runaway. As the temperature approaches its maximum, the ^{22}Mg(p, γ)^{23}Al reaction is balanced by the inverse reaction ^{23}Al(γ,p)^{22}Mg, a result of the low Q-value for photodisintegration, $Q = 0.126$ MeV. This impedance produces an enrichment in ^{22}Mg, which then β-decays to ^{22}Na ($T_{1/2} = 3.86$ s). Reducing the ^{22}Mg abundance (and therefore ^{22}Na) requires a rate for ^{22}Mg(p, γ)^{23}Al that is much higher than expected on the basis of present experimental and theoretical studies of the ^{23}Al level parameters (Wiescher *et al*. 1988*b*). It also requires a strong ^{23}Al(p, γ)^{24}Si reaction (Herndl *et al*. 1995; Schatz *et al*. 1997*b*) to allow the break-out from the ^{22}Mg(p, γ)–^{23}Al(γ,p) equilibrium. A direct measurement of ^{22}Mg(p, γ)^{23}Al and ^{23}Al(p, γ)^{24}Si with radioactive ^{22}Mg and ^{23}Al beams is necessary to clarify the question. However, using presently available nuclear-structure information for ^{23}Al and ^{24}Si, the simulation of nova nucleosynthesis indicates that essentially no flow occurs via ^{22}Mg(p, γ)^{23}Al(p, γ)^{24}Si (Schatz *et al*. 1997*b*).

The production of the long-lived ^{26}Al ($T_{1/2} = 7.16 \times 10^5$ years) in novae takes place via ^{24}Mg(p, γ)^{25}Al($\beta^+\nu$) ^{25}Mg(p, γ)^{26}Al. Figure 8 shows that a substantial amount of ^{26}Al is made at the onset of the runaway. The supply of ^{24}Mg is maintained by the sequence ^{23}Mg(p, γ)^{24}Al($\beta^+\nu$)^{24}Mg and thus the ^{26}Al abundance is tied to the rate for the ^{23}Mg(p, γ)^{24}Al reaction. However, the effect of ^{23}Mg(p, γ) on ^{26}Al is

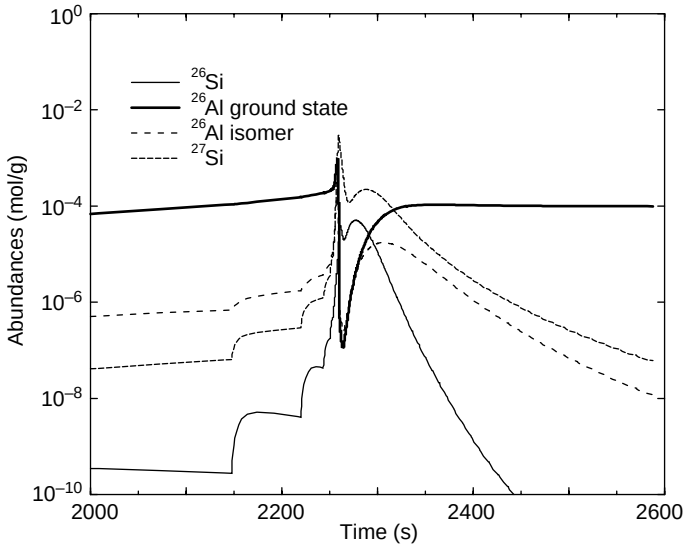

Figure 8. Nucleosynthesis in the hot MgAl cycles in Ne-nova burning. The initial amount of ^{24}Mg is only partly converted to ^{26}Al, but mainly processed via the isomeric state of ^{26}Al*, which subsequently decays to ^{26}Mg.

somewhat counterintuitive. A weak ^{23}Mg(p, γ)^{24}Al reaction does naturally lead to a reduction in the amount of ^{26}Al produced, but the same is true for a strong ^{23}Mg(p, γ) reaction. In the latter case, ^{26}Al is produced earlier in the outburst, and at higher temperatures where it is readily destroyed by the ^{26}Al(p, γ)^{27}Si reaction. A sizeable final abundance of ^{26}Al requires that the ^{23}Mg(p, γ)^{24}Al reaction rate be somewhat smaller than is currently estimated. A recent estimate of the rate is based on the measurement of the excitation energies of the proton unbound states in the compound nucleus ^{24}Al (Kubono *et al*. 1995). The resonance strengths were estimated from the mirror states in ^{24}Na (see also Wiescher *et al*. 1986); careful shell model studies of these levels may therefore improve the present estimates (H. Herndl, personal communication). At higher temperatures, the reaction sequences ^{25}Al(p, γ)^{26}Si(p, γ)^{27}P and ^{25}Al(p, γ)^{26}Si($\beta^+\nu$)^{26}Al*($\beta^+\nu$)^{26}Mg bypass ^{26}Al. The production of long-lived ^{26}Al at nova peak temperature conditions depends therefore sensitively on the reaction rate of ^{25}Al(p, γ)^{26}Si. The reaction rates of ^{25}Mg(p, γ)^{26}Al and ^{25}Al(p, γ)^{26}Si have been recently re-analysed by using all available experimental reaction and structure data (Iliadis *et al*. 1996*a*), but considerable uncertainty remains, particularly for the latter reaction. The rate of the ^{26}Si(p, γ)^{27}P reaction is based on shell-model calculations alone and is therefore also highly uncertain (Herndl *et al*. 1995). A reliable calculation of ^{26}Al nucleosynthesis in novae requires improvements in our knowledge of these rates, and in particular those for the ^{23}Mg(p, γ)^{24}Al and ^{25}Al(p, γ)^{26}Si reactions.

In this discussion, we have recommended measurements of a number of (p, γ) reactions on short-lived targets, in particular ^{22,23}Mg(p, γ), ^{23,25}Al(p, γ), and ^{26}Si(p, γ). Is this a reasonable request? The current state of the art is limited to resonances with strengths greater than several electronvolts, while the resonances in the aforementioned reactions are expected to be much weaker. In addition, many of the relevant resonances are characterized by $\Gamma_{\rm p} \gg \Gamma_\gamma$ and therefore the resonance strengths are

simply proportional to Γ_γ. Good estimates for Γ_γ can, in principle, be obtained from analogue nuclei. In this case, the major uncertainty in the rate may not be in the resonance strength, but in the resonance energy (which enters the rate exponentially). Hence, a possible first step in studying these reactions would be to perform spectroscopic studies designed to measure excitation energies, rather than to attempt a direct (p,γ) measurement. However, reaching the compound nuclei of interest by using stable beams and stable targets is complicated by low cross-sections and selectivity in the final states populated. These limitations could be overcome by using radioactive beams. For example, proton-capture resonances could be populated via $(^3\mathrm{He},\mathrm{d})$ or other transfer reactions in inverse kinematics. The necessary use of inverse kinematics does present some experimental challenges. The heavy recoils will emerge in a tight, forward cone and will be too compressed in energy and angle to be useful in extracting an excitation energy. Although one could tag the reaction of interest by detecting recoils, it is the light ejectiles that will provide the energy information. The direct-reaction amplitude is enhanced when the light particles emerge at back angles in the centre of mass, which implies low energies in the laboratory. Nonetheless, this type of experiment appears to be feasible and should be developed.

Reaction cycles could also occur in the SiP and SCl regions. Strong cycling anywhere along the reaction path would both limit the amount of material transported to heavier masses and give rise to spectral features in the ensuing ejecta. The efficiency of cycling is governed by the temperature-dependent competition between the (p,α) reaction that maintains the cycle and the (p,γ) reaction that breaks it. Although these branch points all occur at stable nuclei, ^{23}Na (Görres *et al*. 1989), ^{27}Al (Champagne *et al*. 1988; Timmermann *et al*. 1989), ^{31}P (Iliadis *et al*. 1993), and ^{35}Cl (Ross *et al*. 1995), uncertainties in the reaction rates still exist, particularly in the α-channels. An alternative to a direct measurement is to measure β-delayed particle decays. The β-delayed α-decay of ^{36}K has recently been measured (Iliadis *et al*. 1996*b*) and the results indicate that, contrary to expectations, a SCl cycle will occur. This is presumably the source of the sulphur lines observed in some Ne-novae.

4. The rp-process during an X-ray burst

The X-ray bursts have been suggested as possible sites for high-temperature hydrogen burning via the rp- and αp-process (Wallace & Woosley 1981; Ayasli & Joos 1982; Woosley & Weaver 1984; Taam 1985, Fujimoto *et al*. 1987; Taam *et al*. 1993). Though they are frequently observed (Lewin *et al*. 1993), the nucleosynthesis and the correlated nuclear energy generation have not been completely inbedded in the models (Schatz *et al*. 1997*a*). The standard models for type-I X-ray bursts are based on accretion processes in a close binary system similar to the nova scenario discussed above, though this case involves accretion onto the surface of a neutron star. Typical predictions for the accretion rate vary between 10^{-10} and $10^{-9} M_\odot\ \mathrm{a}^{-1}$. The accreted matter is continuously compressed by the freshly accreted material until it reaches sufficiently high pressure and temperature to trigger nuclear reactions.

Nuclear burning is ignited at high density, $\rho \geqslant 10^6\ \mathrm{g\,cm}^{-3}$, in the accreted envelope, via the pp-chains, the hot CNO-cycles and the triple-α-process. The released energy produces a thermonuclear runaway under partly degenerate conditions at the base of the accreted layer. Peak temperatures of up to 2×10^9 K can be reached before the degeneracy is completely lifted (Bildsten 1997). These temperatures are

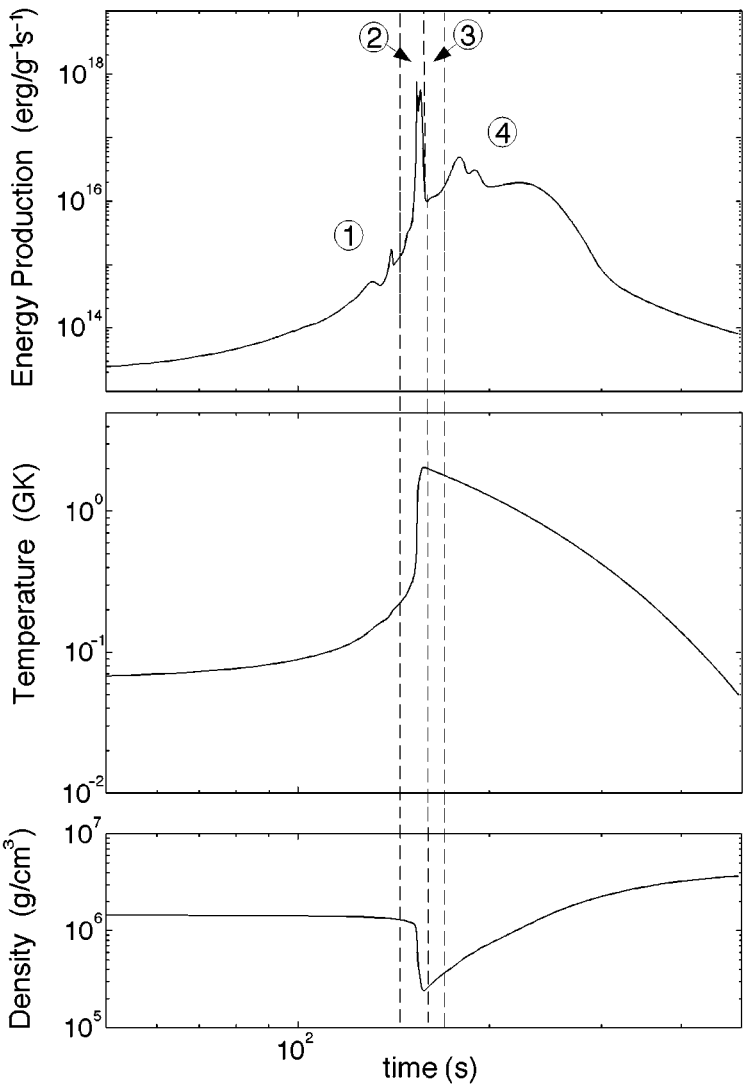

Figure 9. Luminosity, temperature, and density as a function of time for a simplified X-ray-burst model. Indicated are the different phases during the thermonuclear runaway. Phases 1, 2, and 4 correspond to periods of rapid nucleosynthesis, while phase 3 is a dormant period at the maximum of the temperature curve. Further details are discussed in the text.

sufficiently high to trigger the rp- and the αp-process. The energy released by the latter process drives the runaway (Woosley & Weaver 1984; Taam 1985; Fujimoto *et al*. 1987). The time-scale for the thermal runaway and the subsequent cooling phase varies between 10 s and 100 s (Woosley & Weaver 1984), depending on the particular model parameters describing the accretion process. Within this time-scale, the rp-process can proceed up to ^{56}Ni (Wallace & Woosley 1981), and even further in a second burst up to ^{96}Cd (Woosley & Weaver 1984; Wallace & Woosley 1984; Van Wormer *et al*. 1994; Schatz *et al*. 1997*a*).

Figure 9 shows the energy production, temperature and density in the accreted

envelope (burning zone) for a one-zone model. The structure, or the luminosity, clearly shows periods of unimpeded reaction flow where rapid proton and alpha captures and β-decays lead to an increase in energy generation. Also apparent are waiting points, where further proton capture is surpressed (Schatz *et al*. 1997*a*). Here energy production slows. This situation can occur when the Q-value for the next (p,γ) reaction is low, in which case there will be a strong inverse photodisintegration. Waiting points are also encountered when proton capture leads to an isotone that is proton unbound. Further processing must await either the slow β-decay of the waiting-point isotope, an alpha capture (for low-Z isotopes), or a two-proton capture process (high-Z isotopes) (Van Wormer *et al*. 1994; Schatz *et al*. 1997*a*). The latter two possibilities require conditions of high density. The mean time spent at a waiting point is influenced by changes in temperature and density which can affect the (p,γ)–$(\gamma\mathrm{p})$ equilibrium and α-capture rate quite drastically. In addition, the β-decay rate can also be modified (as discussed in § 2 *d*).

The start of the thermonuclear runaway produces a rapid rise in temperature, but the density remains constant since the pressure is still dominated by the pressure of the degenerate electron gas. However, with increasing temperature the ion pressure and the radiation pressure increase dramatically and the gas expands, leading to a decrease in density before the peak temperature is reached. When the cooling rate becomes equal to the energy production rate of $\epsilon_{\mathrm{nucl}} \approx 10^{18}\,\mathrm{erg\,g^{-1}s^{-1}}$ the temperature reaches its peak value of $T \approx 2.5 \times 10^9$ K. At this point the pressure has dropped by approximately one order of magnitude to $\rho \approx 2.5 \times 10^5\,\mathrm{g\,cm^{-3}}$. The decrease in temperature then leads to a corresponding increase in density. The energy production in the burst is characterized by four distinct periods of temperature and density: (1) the ignition phase of the burst, (2) the peak of the burst, (3) the dormant phase of the burst, and (4) the after-burst phase.

Phase (1) is characterized by operation of the hot CNO cycles, triggered by proton-capture reactions of the accreted hydrogen on the carbon, nitrogen, and oxygen isotopes that have not been destroyed by spallation in the outer atmosphere of the accreting neutron star (Bildsten *et al*. 1992). The energy production and the nucleosynthesis are shown in figure 10. The two peaks in the energy production are caused by the conversion of the initial abundance of ^{12}C into ^{14}O, which depends sensitively on the $^{13}\mathrm{N}(\mathrm{p},\gamma)^{14}\mathrm{O}$ rate; and of ^{16}O into ^{15}O by two subsequent proton capture reactions, which depends on the $^{17}\mathrm{F}(\mathrm{p},\gamma)^{18}\mathrm{Ne}$ rate. Because of the slow decay of the ^{14}O and ^{15}O isotopes, the hot CNO cycle stops and the energy production drops. This can also be seen in the reaction flow at the end of this phase (integrated over the duration of the second peak), which is shown in figure 11. The main reaction flow is confined to the CNO cycles, but, as seen in figure 10, the temperature has already increased sufficiently to trigger phase (2) of the burst, the ignition of the triple-α-reaction.

Phase (2) is initiated at a temperature of $T \approx 2.4 \times 10^8$ K via the triple α-process. At the same time, the waiting-point nuclei, ^{14}O, ^{15}O, and ^{18}Ne, are rapidly depleted by α-capture. The reaction rates for the $^{14}\mathrm{O}(\alpha,\mathrm{p})^{17}\mathrm{F}$ (Wiescher *et al*. 1987; Funck & Langanke 1988; Funck *et al*. 1989; Hahn *et al*. 1996) and the $^{15}\mathrm{O}(\alpha,\gamma)^{19}\mathrm{Ne}$ reaction (Langanke *et al*. 1986; Magnus *et al*. 1987, 1990; Mao *et al*. 1995; de Oliveria *et al*. 1997) are the subject of frequent discussions in the literature. The present rates are based on transfer-reaction studies of the compound nuclei and their respective mirrors. A direct measurement with radioactive beams will be extremely difficult

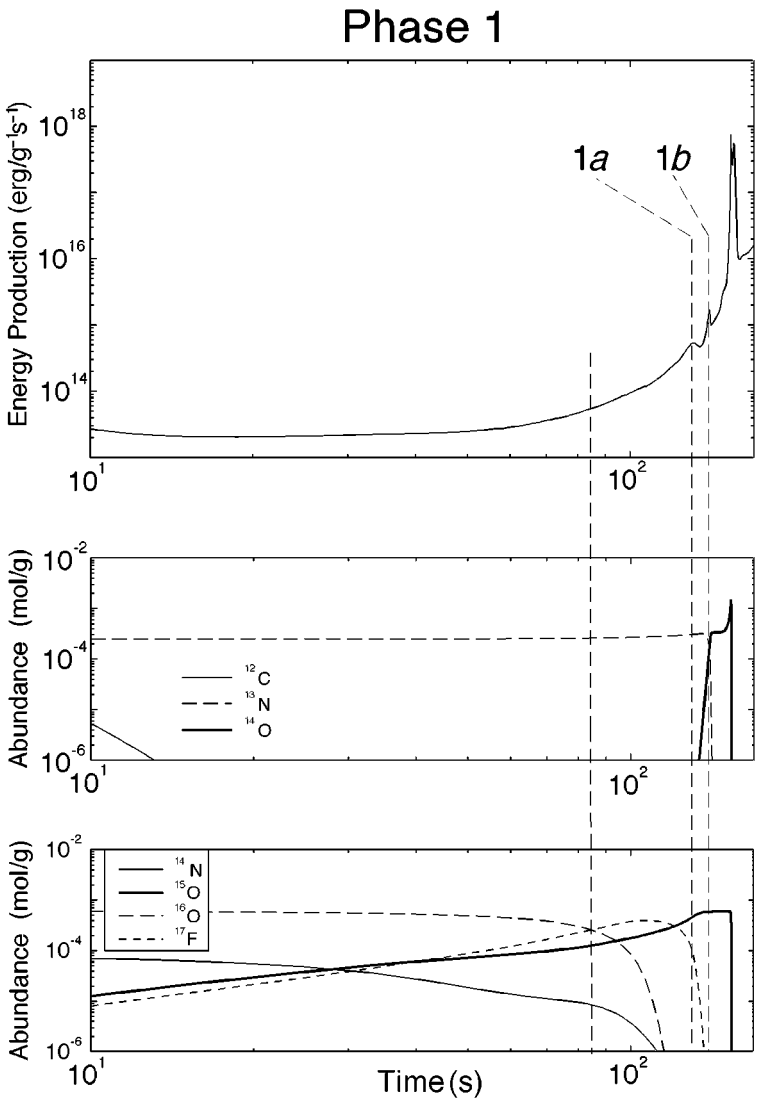

Figure 10. Luminosity and nucleosynthesis in the early phase (1) of an X-ray burst. Peaks 1a and 1b correspond to the burning of ^{13}N and ^{17}F.

because of low cross-sections, the result of Coulomb-barrier inhibition. However, the ground-state branch of $^{14}\mathrm{O}(\alpha,\mathrm{p})^{17}\mathrm{F}$ could be obtained from the inverse reaction $^{17}\mathrm{F}(\mathrm{p},\alpha)^{14}\mathrm{O}$ and preliminary measurements are underway at several laboratories. A similar situation is found for the rate of the $^{18}\mathrm{Ne}(\alpha,\mathrm{p})^{21}\mathrm{Na}$ reaction, which is estimated on the basis of the level structure of the compound nucleus ^{22}Mg (Görres *et al*. 1995*a*). At higher temperatures the estimated rate agrees with Hauser–Feshbach predictions, an attempt is presently being made at Louvain-la-Neuve to study this reaction at higher energies.

The fine structure of the energy burst is characterized by the different waiting points along the process path and is shown in figure 12 together with the abundances

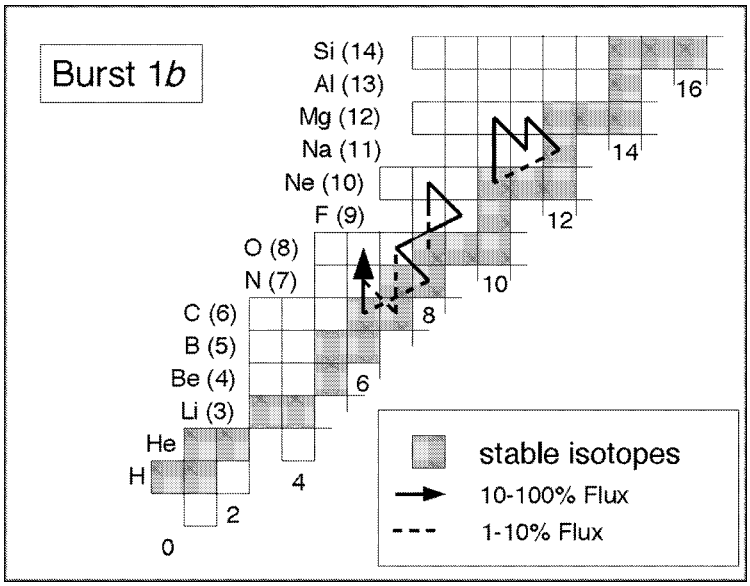

Figure 11. The reaction flow in the early phase (1) of an X-ray burst, which is characterized by the hot CNO cycles and the hot NeNa cycle.

of the most important waiting point nuclei along the process path. During the first burst (2a) the waiting-point isotopes ^{14}O, ^{15}O, and ^{18}Ne, that were produced by the hot CNO cycles, are rapidly converted by the αp-process to ^{24}Si. Because further reactions must wait for the β-decay of ^{24}Si ($T_{1/2} = 102$ ms), energy production drops until higher temperatures initiate proton and α captures leading to the production of the next waiting point isotopes, ^{29}S (2b) and ^{34}Ar (2c). The rapid increase in temperature allows subsequent α-captures to bridge these waiting points, which leads ultimately to ^{56}Ni (2d). Because most of the reaction path is characterized by (α, p) reactions, considerably more helium is burned than hydrogen. This has the effect of converting the accreted helium to ^{56}Ni. However, most of these reaction rates are estimated from Hauser–Feshbach calculations and require experimental verification. The reaction flow, integrated over the duration of the last phase (2d) of the burst is shown in figure 13. At this point, peak temperatures of $T \approx 2.5 \times 10^9$ K have been reached and further processing is halted by a $^{56}\mathrm{Ni}(\mathrm{p},\gamma)$–$(\gamma,\mathrm{p})$ equilibrium (Schatz *et al*. 1997*a*). As a result, energy production drops rapidly while most of the initial inventory of heavy isotopes as well as a large fraction of the initial helium remains stored in the waiting point nucleus ^{56}Ni. The drop in energy production slows the temperature growth rate just before the peak temperature is reached.

Further progress depends critically on the reaction rates for $^{56}\mathrm{Ni}(\mathrm{p},\gamma)^{57}\mathrm{Cu}$ and the subsequent proton capture, $^{57}\mathrm{Cu}(\mathrm{p},\gamma)^{58}\mathrm{Zn}$. The present rates are rather uncertain. In the case of $^{56}\mathrm{Ni}(\mathrm{p},\gamma)^{57}\mathrm{Cu}$ they are based mainly on measurements of the level structure of ^{57}Cu (Sherrill *et al*. 1985; Van Wormer *et al*. 1994; Zhou *et al*. 1996), though there is an ongoing programme to measure them with a radioactive ^{56}Ni beam (Rehm *et al*. 1997). Nothing is known about the level structure in ^{58}Zn and the present rate for $^{57}\mathrm{Cu}(\mathrm{p},\gamma)^{58}\mathrm{Zn}$ is based solely on Hauser–Feshbach calculations. Because the level density may not be high enough to justify this treatment, more experimental data would be appreciated.

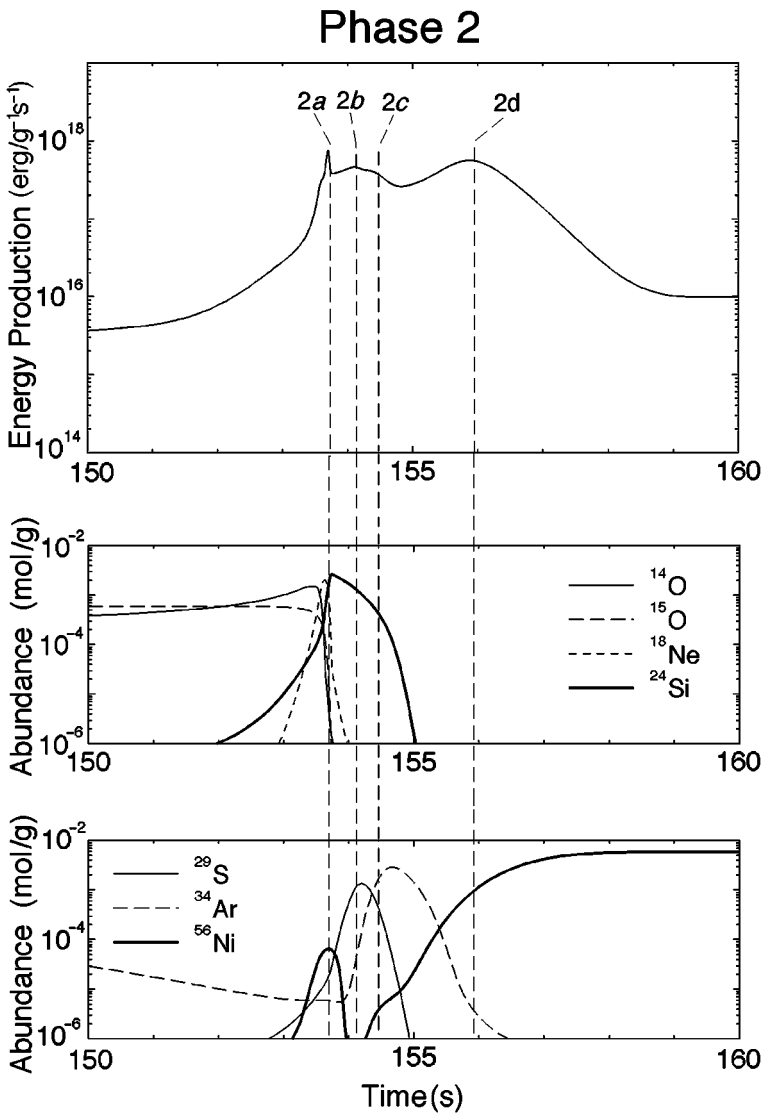

Figure 12. Peak conditions in the energy production of the X-ray burst. The structure of the energy-generation curve is determined by the waiting point characteristics of the rp-process. Further details may be found in the text.

At temperatures above *ca.* 2×10^9 K, both ^{56}Ni(p, γ)^{57}Cu and ^{57}Cu(p, γ)^{58}Zn are in equilibrium with the inverse photodisintegration. Therefore, the reaction flow halts, the energy production ceases causing a rapid drop in luminosity and subsequently a slow decrease in temperature. This cooling period corresponds to the dormant phase (3) of the burst, where further processing awaits the decay of ^{56}Ni.

The effective lifetime of ^{56}Ni depends on the cooling rate in the accreted envelope, as soon as the temperature has dropped below *ca.* 2×10^9 K the effective lifetime of ^{56}Ni decreases drastically because the ^{57}Cu(p, γ)–^{58}Zn(γ, p) equilibrium is lifted and two-proton capture on ^{56}Ni occurs (Schatz *et al.* 1997*a*). This initiates phase

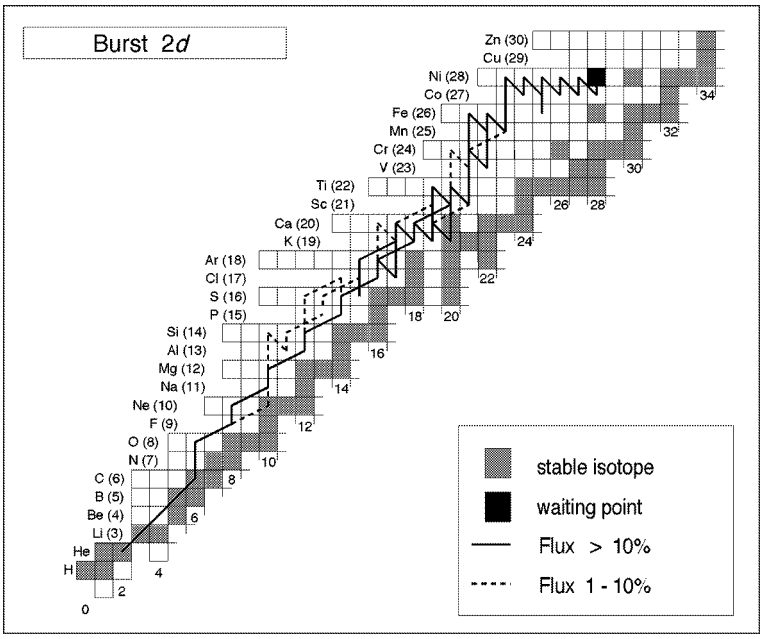

Figure 13. The αp- and rp-process reaction path in the thermonuclear runaway phase (2) of the X-ray burst.

(4) of the energy burst, which is characterized by nucleosynthesis via the rp-process beyond ^{56}Ni.

Figure 14 shows the details of the burst structure in the cooling phase. The peaks in the energy production are caused by the depletion of ^{56}Ni and the further processing towards the waiting point ^{64}Ge, and by subsequent nucleosynthesis towards ^{68}Se. In the final phase, the waiting point ^{68}Se is converted to heavier isotopes in the mass 100 region.

Within this phase, the rp-process path runs along the $N = Z$ line which merges with the drip-line at around $Z = 32$ (Schatz *et al.* 1997*a*). This raises the question of where the rp-process terminates (Wallace & Woosley 1985). It has been argued that long-lived $N = Z$ even–even nuclei like ^{64}Ge ($T_{1/2} = 90$ s) might represent an endpoint for the rp-process nucleosynthesis if the neighbouring $T_Z = 1/2$ nucleus $(Z + 1, N)$ (^{65}As) is proton unbound. The process would have to wait for the β-decay of the long-lived isotope, and this time delay might possibly exceed the short macroscopic time-scale for the high-temperature and density conditions in the thermal runaway. However, it has been shown that the lifetime of ^{65}As is sufficiently long (Mohar *et al.* 1991; Winger *et al.* 1993) so that the isotope is most likely particle bound or unbound only by *ca.* 450 keV. In this case, the lifetime is determined by the proton penetrability (Winger *et al.* 1993). Independent heavy-ion fragmentation experiments at the Michigan State A1200 mass separator and at the GANIL LISE separator indicate that ^{69}Br and ^{73}Rb are most likely unbound because they were not observed at the focal plane detector of the respective mass separator (Mohar *et al.* 1991; Blank *et al.* 1995; Pfaff *et al.* 1996). These observations limit the lifetimes of these isotopes to be less than the flight time through the separator ($T_{1/2} \leqslant 150$ ns). Such a short lifetime indicates that these two isotopes

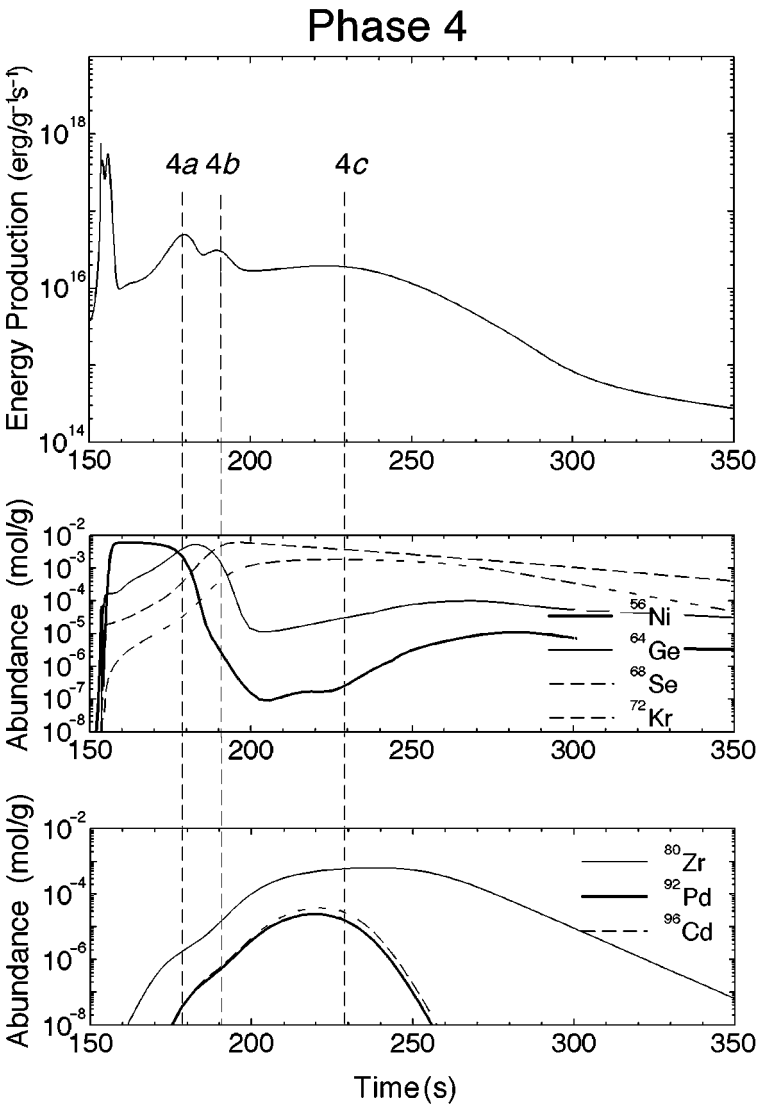

Figure 14. Luminosity and nucleosynthesis in the late phase (4) of an X-ray burst. The peaks in the luminosity correspond to the destruction of waiting-point nuclei.

are most likely proton unbound. It was therefore proposed that ^{68}Se ($T_{1/2} = 35$ s) and ^{72}Kr ($T_{1/2} = 17$ s) are the most likely candidates for endpoints of rp-process nucleosynthesis (Blank *et al*. 1995; Pfaff *et al*. 1996). However, because of the odd–even effects in nuclear binding energies, the two $T = 1$ even–even nuclei, ^{70}Kr and ^{74}Sr have been predicted to be bound by all mass model calculations (Jänecke & Masson 1988; Aboussir *et al*. 1992; Möller *et al*. 1995). This prediction has been verified in recent GANIL experiments (Regan *et al*. 1997). For these conditions it is expected (Schatz *et al*. 1997*a*) that two-proton capture processes like ^{68}Se$(2\mathrm{p},\gamma)^{70}$Kr and ^{72}Kr$(2\mathrm{p},\gamma)^{74}$Sr are sufficiently fast to bypass the comparatively slow β-decay, provided that ^{69}Br and ^{73}Rb are unbound by less than *ca.* 1 MeV. If this is the case,

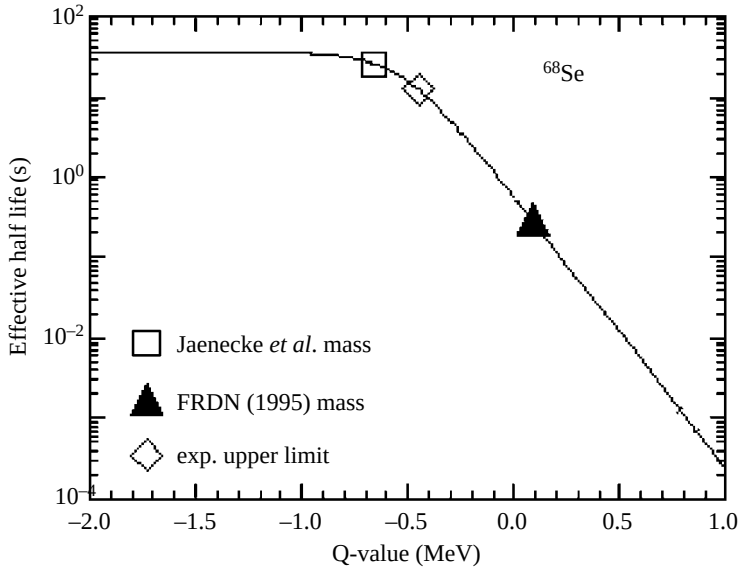

Figure 15. The effective half-life of ^{68}Se at a temperature of 1.5 GK and a density of 10^6 g cm^{-2} for β-decay and for the two-proton capture process as a function of the Q-value for the ^{69}Br(p, γ)^{70}Kr. Also indicated are theoretical predictions from mass-model calculations as well as the experimental upper limit for the Q-value.

then the effective lifetime of ^{68}Se, ^{72}Kr will be significantly reduced at high densities. Figure 15 indicates the effective lifetime for ^{68}Se as a function of the Q-value for the subsequent proton capture process at a temperature of 1.5×10^9 K and a density of $\rho = 10^6$ g cm^{-3}. Figure 16 shows the reaction flow integrated over the duration of (4d). Notice that the αp-process is only dominant below sulphur, a result of the decrease in the initial ^{4}He abundance. At higher masses, the reaction path is characterized by the rp-process pattern leading up to ^{100}Sn. In the final phase, most ($\geqslant$90%) of the initial helium as well as most of the other isotopes are converted to heavy isotopes with masses $A \geqslant 72$. Therefore, it is of interest to consider the relative abundance distribution in this mass range during the final phase of the X-ray burst. While the question of possible mass loss accompanying an X-ray burst requires more sophisticated models than are presently available, it is nevertheless of interest to study the abundance distribution in the accreted material after the thermal runaway. If they eject mass, X-ray bursts may contribute to the observed abundance distribution. If mass loss is prevented by the gravitational potential of the neutron star, then the freshly synthesized nuclei may become seed material for processes triggered by the formation of neutrons via electron capture on the remaining hydrogen in the high-density zones ($\rho \geqslant 10^7$ g cm^{-3}) (Taam *et al.* 1996).

Figure 17 shows the abundance distribution in the material after the thermonuclear runaway freezes out, i.e. when all of the β-unstable isotopes along the process path have decayed back to the line of stability. While there is still an appreciable amount of hydrogen, the bulk of the material has been converted to nuclei with masses $A \geqslant 70$. Figure 18 shows a comparison with solar abundances. It is apparent that all the isotopes above mass $A = 68$ are enriched by more than five orders of magnitude as compared with the solar abundances that served as the initial distribution of

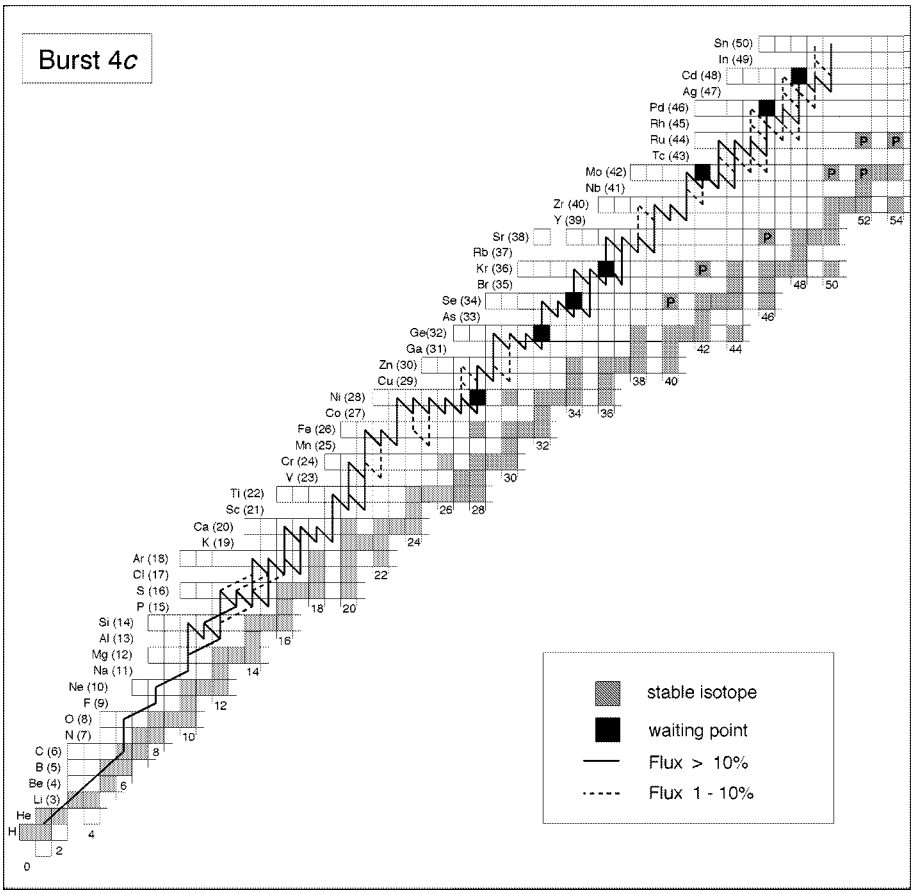

Figure 16. The reaction flux in the late phase (4d) of the X-ray burst. The overall flux is dominated by the rp-process. Only the lowest-Z nuclei ($Z \leqslant 14$) is the Coulomb barrier low enough for α-capture reactions to compete with the proton capture and the β-decay.

the accreted material. Particularly abundant are the light p-nuclei ^{74}Se, ^{78}Kr, ^{84}Sr, ^{92}Mo, ^{94}Mo, ^{96}Ru, ^{98}Ru (Lambert 1992), which are enriched by approximately seven orders of magnitude compared to their solar abundances. This is noteworthy because the relatively high observed abundances for these isotopes have not been explained by classical p-process scenarios (Woosley & Howard 1990; Rayet *et al*. 1990, 1995; Howard *et al*. 1991), or by neutrino-induced reactions processes in type II supernovae (Hoffman *et al*. 1996). If a sufficent mass can escape the gravitational potential of the neutron star, X-ray bursts may be a potential source for these isotopes.

5. Nucleosynthesis in supernovae

Supernova events can be triggered by the nuclear detonation of a white dwarf (type Ia), or by the core collapse of a massive star (type Ib or type II). Although a full treatment of supernova nucleosynthesis is beyond the scope of this article, we will highlight some aspects of this complex topic by focusing on processes occurring deep within a type II event. In these environments, nuclear interactions can occur

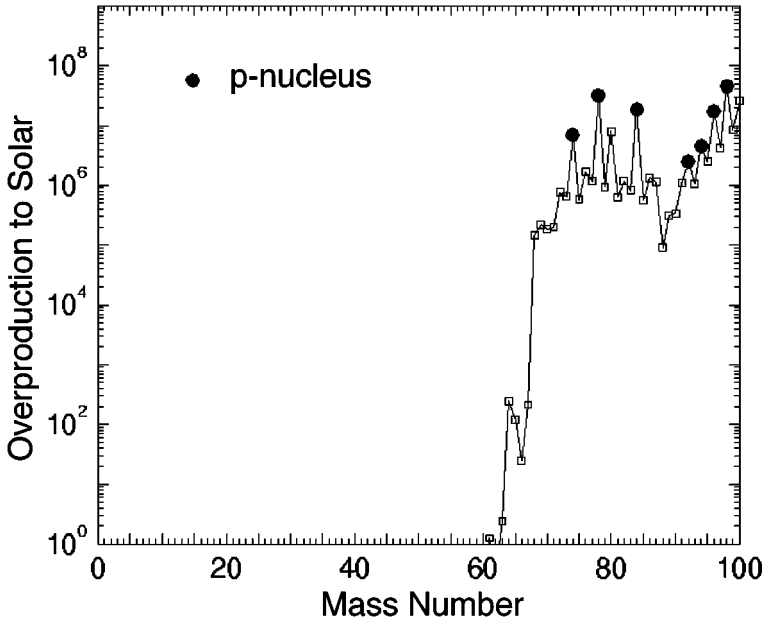

Figure 17. The abundance distribution after the thermonuclear runaway of a single X-ray burst.

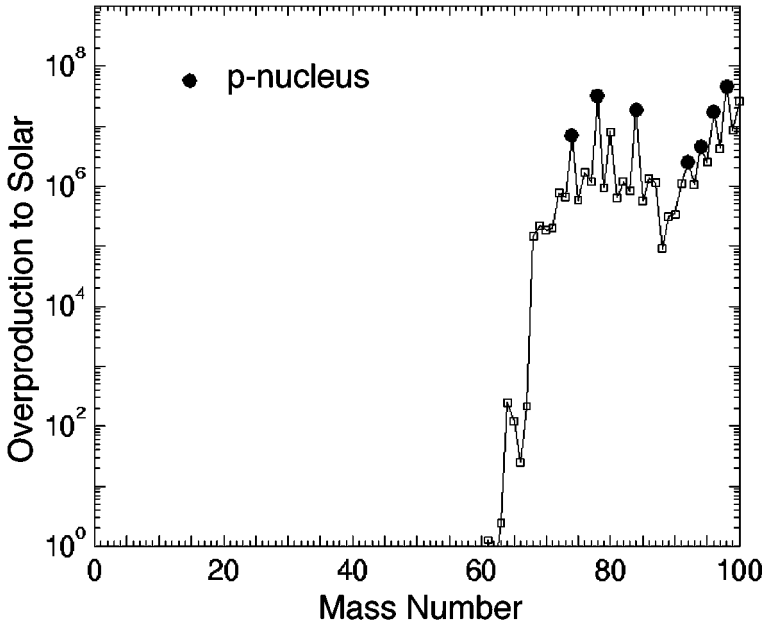

Figure 18. The ratio of the produced abundances and the initial solar abundances after the thermonuclear runaway of a single X-ray burst. The light p-nuclei are marked as black dots, their overabundance is about one to two orders of magnitude larger than the of other isotopes. The abundances of the last two mass numbers are not reliable because they correspond to the end of the network.

under conditions approaching equilibrium and entropy replaces the reaction rate as the quantity that describes the evolution of the system. Nuclear burning can then be described as a process whereby the system tries to maximize its entropy subject to some local constraints. The task for nuclear physics is to provide the global information needed to describe this quasi-equilibrium condition.

The last stage of core nucleosynthesis within a massive star produces elements in the iron region, also under quasi-equilibrium conditions. Once this point is reached, exoergic nuclear reactions cease and degenerate electrons provide the primary source of outward pressure (Arnett 1996). However, electron capture rapidly robs the core of this support and collapse quickly ensues. As the density rises, neutrino interactions will also come into play. Describing this core-collapse phase to first order requires a knowledge of weak-interaction strengths.

Both Fermi (F) and Gamow–Teller (GT) transitions can regulate the behaviour of the collapsing core. However, the F strength is concentrated in the isobaric-analogue state (IAS), which is often located too high in energy to be of importance. An exception to this is found in the post-collapse phase where energetic neutrinos can populate the IAS (McLaughlin & Fuller 1995). Thus, we are primarily interested in the GT-part of the interaction, and in particular, the distribution of GT strength as a function of energy. The cases of immediate interest involve $T_< \rightarrow T_>$ transitions and n-rich nuclei in the sd and fp shells since heavier nuclei are initially blocked (Fuller 1982). Neutrino capture involves $T_> \rightarrow T_<$ transitions. Although the most direct way to determine GT strengths is through β-decay measurements, most of the strength distribution is kinematically inaccessible. Therefore, indirect techniques have been developed, based upon measurements of charge-exchange reactions. In this approach, electron and antineutrino capture can be probed via an (n,p) reaction while (p,n) is used to treat neutrino capture. The reaction kinematics are defined in such a way that the isovector spin-flip part of the NN interaction is predominant. This requires bombarding energies in excess of 100 MeV and detection of outgoing particles at angles $\theta \approx 0^\circ$. In this regime, the charge-exchange operator resembles that for β-decay (Goodman *et al*. 1980; Taddeucci *et al*. 1987), and the correspondence between the measured cross-section and the reduced transition strength B(GT) can be obtained by comparing charge-exchange data with β-decay (Goodman *et al*. 1980; Taddeucci *et al*. 1982, 1987). A large number of (p,n) and (n,p) results have been reported and a general feature is that the observed strength is lower than predicted. From comparisons with β-decay, it appears that B(GT) can be extracted to an accuracy of better than 20–30% for strong, low-lying transitions (Sugarbaker 1995). Some problems may exist for weak and/or high-lying states (see, for example, Garcia *et al*. 1995).

All of the measurements in the mass region of interest for supernovae have involved stable targets and thus calculated rates are used for short-lived nuclei. Although more work is necessary in order to improve the reliability of theoretical strength distributions, it is possible to extend the experimental database by using radioactive beams in inverse kinematics. A measurement of the ^{1}H(^{6}He, ^{6}Li)n reaction at $E(^6\mathrm{He}) = 93$ MeV amu^{-1} has recently been reported (Brown *et al*. 1996). Note that only (p,n) reactions can be measured in this manner because the (n,p) direction would require a neutron target or a heavy-ion reaction. On the other hand, a wide variety of beams can be produced via projectile fragmentation and it is expected that this will be an area of increasing activity.

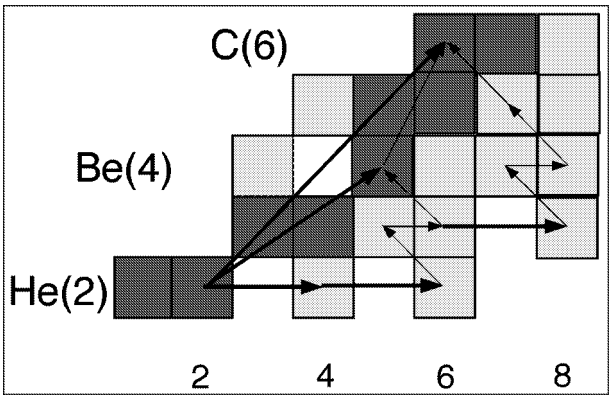

Figure 19. Shown are the various three-particle-induced reaction sequences (thick arrows) which allow recombination of free ^{4}He to ^{12}C at the conditions of an α-rich freeze out. The dark shaded area indicates the stable isotopes, the light shaded areas indicate particle stable, but β-unstable isotopes.

After the core collapses and rebounds, a shock wave propagates through the material surrounding the nascent neutron star. Neutrino heating occurs in the wake of the shock front (Wilson & Mayle 1988, 1993). Under these conditions, baryonic matter achieves a quasi-equilibrium at high entropy in which free α-particles, protons, and neutrons are favoured with a high photon-to-baryon ratio (Woosley *et al*. 1973). In the subsequent expansion phase, which is driven by the neutrino-induced shock, recombination of the α-particles is constrained by slow three-particle interactions such as the triple α reaction, $^4\mathrm{He}(2\alpha,\gamma)^{12}\mathrm{C}$, and the reaction sequence $^4\mathrm{He}(\alpha\mathrm{n},\gamma)^9\mathrm{Be}(\alpha,\mathrm{n})^{12}\mathrm{C}$ that bridge the mass 5 and mass 8 gap, as shown in figure 19. Once the α-particles have recombined, more massive nuclei are quickly assembled in an 'α-rich freeze-out' (Woosley & Hoffman 1992) which is governed by the rates for expansion and cooling as well as by the rates for converting ^{4}He to ^{12}C.

The charged-particle reactions are the first to fall out of equilibrium as the hot bubble rapidly expands. This leaves free neutrons and nuclei as seed material for a rapid neutron-capture process, named the r-process. The path of the r-process and the resulting elemental abundances depend in part on the entropy and the electron fraction. Together, these quantities determine the neutron-to-seed ratio and the isotopic distributions of the seed nuclei. The evolution of temperature and density with time will regulate the various stages of equilibrium behaviour that appear to be reflected in the observed distribution of r-process nuclei. The challenge for nuclear astrophysics is to make the connection between the observed abundances and the astrophysical environment.

From a nuclear-physics perspective, the r-process can be described in terms of equilibria. The reaction path is first determined by an (n,γ)–(γ,n) equilibrium (Cowan *et al*. 1991; Kratz *et al*. 1993), where along a given isotopic chain, the relative abundances are fixed by the neutron-separation energies. A high separation energy favours an (n,γ) reaction and a low relative abundance for that particular nucleus. Once a neutron shell is filled, the separation energy drops and the equilibrium swings in the direction of (γ,n). This impedes further flow and produces large abundances in the region of the shell closure. Following freeze-out, this material will β-decay back to stability, producing the observed r-process abundance peaks. The measured abun-

dances and half-lives also point to the existence of a β-flow equilibrium (Kratz *et al.* 1988), in which the abundances along a given β-decay chain are determined by the half-lives. As the material expands and the density drops, neutron capture decouples and photodisintegration drives the reaction path closer to the line of stability. The final stage of freeze-out involves β decays and β-delayed neutron decays back to stability.

Since the r-process achieves equilibrium conditions, the composition of the seed nuclei is less important than the overall seed abundance. Therefore, we are most interested in the slow reactions at the onset of α recombination. In addition to the $^4\mathrm{He}(2\alpha,\gamma)^{12}\mathrm{C}$ and the $^4\mathrm{He}(\alpha\mathrm{n},\gamma)^9\mathrm{Be}$ reactions, the mass 5 and 8 gaps can also be bridged by reactions that take advantage of the high neutron density that is also present in the gas. These include the reaction sequence $^4\mathrm{He}(2\mathrm{n},\gamma)^6\mathrm{He}(2\mathrm{n},\gamma)^8\mathrm{He}$, etc. (Görres *et al.* 1995*b*; Efros *et al.* 1996). Figure 19 shows the various three-particle reactions that ultimately lead to to heavier nuclei. The cross-sections for these two-neutron captures are significant because of the pronounced halo structure in the ^{6}He and ^{8}He compound systems. Similar enhancements may also occur for other neutron-rich halo nuclei (e.g. for $^9\mathrm{Li}(\mathrm{n},\gamma)^{10}\mathrm{Li}(\mathrm{n},\gamma)^{11}\mathrm{Li}$) (Görres *et al.* 1995*b*). Certainly, the reaction rate depends strongly on the wavefunctions for the halo orbitals, and these can be probed with radioactive beams. For example, beams of halo nuclei could be produced for measurements of Coulomb excitation or Coulomb break-up.

Calculations of r-process nucleosynthesis, using theoretical masses and half-lives, do a very good job of reproducing the gross features of the observed abundance pattern. However, the mass models currently used predict a rather drastic reduction in the neutron-separation energies at the closed shells and this leads to discrepancies in the predicted abundances (Kratz *et al.* 1993; Thielemann *et al.* 1994; Chen *et al.* 1995; Kratz 1995). New calculations, using spherical masses with quenched shell effects, provide much improved fits (Pfeiffer *et al.* 1997). The task is now to construct a realistic, deformed mass model. Since mass models are not designed to extrapolate to new mass regions, it would be highly desirable to extend the database of measured masses for neutron-rich nuclei. More accessible, but equally important are half-lives and decay properties which can be measured with even low beam fluxes by using an isotope separator. Although the intensity of the radioactive beam is not a critical issue, the ability to produce very neutron-rich nuclei is and this will require improvements in the intensity of the primary beam. Detailed experimental investigations of the r-process must await advancements in the technology of radioactive beams.

6. Conclusion

Experimental nuclear astrophysics has proven itself to be a very powerful tool for understanding stellar processes. Combined with observational data, it has allowed us to peek into the stellar interior and to describe the events in a star's life. Up to now, these studies have been limited to the slow reactions on stable nuclei that give the stars their long lifetimes. However, the key to understanding the cataclysmic explosions that we observe in the Milky Way and in distant galaxies is the ability to study nuclear reactions far from stability. Radioactive-beam facilities have offered us the unique opportunity to probe these spectacular events. The present information is sketchy and incomplete, but technical advancements will allow us to gain a better understanding of stellar explosions and explosive nucleosynthesis.

References

Aboussir, Y., Pearson, J. M., Dutta, A. K. & Tondeur, F. 1992 *Nucl. Phys.* A **549**, 155.

Anders, E. & Grevesse, M. 1989 *Geochim. Cosmochim. Acta* **53**, 197.

Arnett, D. A. 1996 *Supernovae and nucleosynthesis*. Princeton University Press.

Ayasli, A. & Joos, P. 1982 *Astrophys. J.* **256**, 637.

Bahcall, J. N. 1962 *Phys. Rev.* **126**, 1143.

Bahcall, J. N. 1964 *Astrophys. J.* **139**, 318.

Becker, H. W., Buchmann, L., Görres, J., Kettner, K. U., Kräwinkel, H., Rolfs, C., Schmalbrock, P., Trautvetter, H. P. & Vlieks, A. 1982 *Nucl. Instrum. Meth.* **198**, 277.

Bildsten, L., Salpeter, E. E. & Wassermann, I. 1992 *Astrophys. J.* **384**, 143.

Bildsten, L. 1997 In *The many faces of neutron stars* (ed. A. Alpar, L. Buccheri & J. van Paradijs). Dordrecht.

Bittner, G., Kretschmer, W. & Schuster, W. 1979 *Nucl. Instrum. Meth.* **167**, 1.

Blank, B. (and 17 others) 1995 *Phys. Rev. Lett* **74**, 4611.

Brown, J. A. (and 12 others) 1996 *Phys. Rev.* C **54**, R2105.

Burbidge, E. M., Burbidge, G., Fowler, W. A. & Hoyle, F. 1957 *Rev. Mod. Phys.* **29**, 547.

Cameron, A. G. W. 1959 *Astrophys. J.* **130**, 452.

Caughlan, G. R. & Fowler, W. A. 1988 *At. Data Nucl. Data Tab.* **40**, 284.

Champagne, A., Cella, C. H., Kouzes, R. T., Lowry, M. M., Magnus, P. V., Smith, M. S. & Mao, Z. Q. 1988 *Nucl. Phys.* A **487**, 433.

Chen, B., Dobaczewski, J., Kratz, K.-L., Kanganke, K., Pfeiffer, B., Thielemann, F. K. & Vogel, P. 1995 *Phys. Lett.* B **355**, 37.

Coc, A., Mochkovitch, R., Oberto, Y., Thibaud, J.-P. & Vangioni-Flam, E. 1995 *Astr. & Astrophys.* **299**, 479.

Cosner, K. & Truran, J. W. 1981 *Astrophys. Space Sci.* **78**, 85.

Coszach, R. (and 22 others) 1995 *Phys. Lett.* B **353**, 184.

Cowan, J. J., Thielemann, F. K. & Truran, J. W. 1991 *Phys. Rep.* **208**, 268.

Decrock, P. (and 14 others) 1991 *Phys. Rev. Lett.* **67**, 808.

de Oliveira, F. (and 16 others) 1997 *Phys. Rev.* C **55**, 3149.

Efros, V. D., Balogh, W., Herndl, H., Hofinger, R. & Oberhummer, H. 1996 *Z. Phys.* A **355**, 101.

Fowler, W. A. 1984 *Rev. Mod. Phys.* **56**, 159.

Fowler, W. A., Caughlan, G. R. & Zimmerman, B. A. 1967 *A. Rev. Astr. Astrophys.* **5**, 525.

Fowler, W. A., Caughlan, G. R. & Zimmerman, B. A. 1975 *A. Rev. Astr. Astrophys.* **13**, 69.

Fujimoto, M., Sztajno, M., Lewin, W. & van Paradijs, J. 1987 *Astrophys. J.* **319**, 902.

Fuller G. 1982 *Astrophys. J.* **252**, 741.

Fuller, G., Fowler, W. A. & Newman, M. J. 1980 *Ap. J. Suppl.* **42**, 447.

Funck, C. & Langanke, K. 1988 *Nucl. Phys.* A **480**, 188.

Funck, C., Grund, B. & Langanke, K. 1989 *Z. Phys.* A **332**, 109.

Galster, W. *et al*. 1991 *Phys. Rev.* C **44**, 2776.

Garcia, A., Adelberger, E. G., Magnus, P. V., Markoff, D. M., Swartz, K. B., Smith, M. S., Hahn, K. I., Bateman, N. & Parker, P. D. 1991 *Phys. Rev.* C **43**, 2012.

Garcia, A., Adelberger, E. G., Magnus, P. V., Swanson, H. E., Wells, D. P., Wietfeldt, F. E., Tengblad, O. & ISOLDE Collaboration 1995 *Phys. Rev.* C **51**, 439.

Glasner, S. A., Livne, E. & Truran, J. W. 1997 *Astrophys. J.* **475**, 754.

Goodman, C. D., Goulding, C. A., Greenfield, M. B., Rapaport, J., Bainum, D. E., Foster, C. C., Love, W.G. & Petrovich, F. *et al*. 1980 *Phys. Rev. Lett.* **44**, 1755.

Görres, J., Kettner, K.U., Kräwinkel, H. & Rolfs, C. 1980 *Nucl. Instrum. Meth.* **177**, 295.

Görres, J., Becker, H. W., Krauss, A., Redder, A., Rolfs, C. & Trautvetter, H. P. 1985 *Nucl. Instrum. Meth.* **241**, 334.
Görres, J., Wiescher, M. & Rolfs, C. 1989 *Astrophys. J.* **343**, 365.
Görres, J., Wiescher, M. & Thielemann, F. K. 1995*a* *Phys. Rev.* C **51**, 392.
Görres J., Herndl, H., Thompson, I. J. & Wiescher, M. 1995*b* *Phys. Rev.* C **52**, 2231.
Graulich, J. S. (and 18 others) 1997 *Nucl.Phys.* A **626**, 751.
Hahn, K. I. (and 21 others) 1996 *Phys. Rev.* C **54**, 1999.
Hansen, C. J. & Kawaler, S. D. 1994 *Stellar interiors*. New York: Springer.
Herndl, H., Görres, J., Wiescher, M., Brown, B. A. & Van Wormer, L. 1995 *Phys. Rev.* C **52**, 1078.
Hilgemeier, M., Becker, H. W., Rolfs, C., Trautvetter, H. P. & Hammer, J. 1988 *Z. Phys.* A **329**, 243.
Hoffman, R. D., Woosley, S. E., Fuller, G. M. & Meyer, B. S. 1996 *Astrophys. J.* **460**, 478.
Howard, W. M., Meyer, B. S. & Woosley, S. E. 1991 *Astrophys. J.* **373**, L5.
Iliadis, C., Görres, J., Ross, J. G., Scheller, K. W., Wiescher, M., Grama, C., Schange, T., Trautvetter, H. P. & Evans, H. 1993 *Nucl. Phys.* A **559**, 83.
Iliadis, C., Buchmann, L., Endt, P. M., Herndl, H. & Wiescher, M. 1996*a* *Phys. Rev.* C **53**, 475.
Iliadis, C., Azuma, R. E., Buchmann, L., Chow, J., D'Auria, J. M., Dombsky, M., Giesen, U., King, J. D. & Morton, A. C. 1996*b* *Nucl. Phys.* A **609**, 237.
Iwasa, N. (and 22 others) 1996 *J. Phys. Soc. Jap.* **65**, 1256.
Iyudin, I. (and 12 others) 1995 *Astr. Astrophys.* **300**, 422.
Jänecke, J. & Masson, P. 1988 *At. Data. Nucl. Data. Tab.* **39**, 265.
Jose, J., Hernanz, M. & Coc, A. 1997 *Astrophys. J. Lett.* **479**, L55.
Jung, M. (and 19 others) 1993 *Nucl. Phys.* A **553**, 309c.
Käppeler, F., Beer, H. & Wisshak, K. 1989 *Rep. Prog. Phys.* **52**, 945.
Kiener, J. (and 19 others) 1993 *Nucl. Phys.* A **552**, 66.
Kratz, K.-L. 1995 *Nuclei in the cosmos III* (ed. M. Busso, R. Gallino & C. M. Raiteri). AIP Conference Proceedings, vol. 327, pp. 113.
Kratz, K.-L., Thielemann, F.-K., Hillebrandt, W., Möller, P., Harms, V., Wöhr, A. & Truran, J. W. 1988 *J. Phys.* G (Suppl.) **14**, 331.
Kratz, K.-L., Bitouzet, J.-P., Thielemann, F.-K., Möller, P. & Pfeiffer, B. 1993 *Astrophys. J.* **403**, 216.
Kubono, S., Kajino, T. & Kato, S. 1995 *Nucl. Phys.* A **588**, 521.
Lambert, D. L. 1992 *Astr. Astrophys. Rev.* **3**, 201.
Langanke, K., Wiescher, M., Fowler, W. A. & Görres, J. 1986 *Astrophys. J.* **301**, 629.
Law, W. Y. & Ritter, H. 1983 *Astr. Astrophys.* **63**, 265.
Leising, M. D. & Clayton, D. D. 1987 *Astrophys. J.* **323**, 159.
Lewin, W., van Paradijs, J. & Taam, R. 1993 *Space Sci. Rev.* **62**, 233.
Livio, M. & Truran, J. W. 1994 *Astrophys. J.* **425**, 797.
Magnus, P. V., Smith, M. S., Parker, P. D., Azuma, R. E., Campell, C., King, J. D. & Vise, J. 1987 *Nucl. Phys.* A **470**, 206.
Magnus, P. V., Smith, M. S., Howard, A. J., Parker, P. D. & Champagne, A. 1990 *Nucl. Phys.* A **506**, 332.
Mao Z. Q., Fortune, H. T. & Lacaze, A. G. 1995,*Phys. Rev. Lett.* **74**, 3760.
Marion, J. B. & Fowler, W. A. 1957 *Astrophys. J.* **125**, 221.
McLaughlin, G. C. & Fuller, G. M. 1995 *Astrophys. J.* **455**, 202.
Mohar M. F., Bazin, D., Benenson, W., Morrissey, D. J., Orr, N. A., Sherrill, B. M., Swan, D., Winger, J. A., Mueller, A. C. & Guillemaud-Mueller, D. 1991 *Phys. Rev. Lett* **66**, 1571.
Möller, P., Nix, J. R., Myers, D. & Swiatecki, W. J. 1995 *At. Data. Nucl. Data. Tab.* **59**, 185.

Motobayashi, T. (and 19 others) 1991 *Phys. Lett.* B **264**, 259.

Pfaff, R., Morrissey, D. J., Benenson, W., Fauerbach, M., Hellström, M., Powell, C. F., Sherrill, B. M., Steiner, M. & Winger, J. A. 1996 *Phys. Rev.* C **53**, 1753.

Pfeiffer, B., Kratz, K.-L. & Thielemann, F.-K. 1997 *Z. Phys.* A **357**, 235.

Politano, M., Starrfield, S., Truran, J. W., Sparks, W. M. & Weiss, A. 1995 *Astrophys. J.* **448**, 807.

Prantzos, N. & Diehl, R. 1995 *Phys. Rep* **267**, 1.

Rauscher, T., Kratz, K.-L. & Thielemann, F.-K. 1997 *Phys. Rev.* C **56**, 1613.

Rayet, M., Prantzos, N. & Arnould, M. 1990 *Astr. Astrophys.* **227**, 271.

Rayet, M., Arnould, M., Hashimoto, M., Prantzos, N. & Nomoto, K. 1995 *Astr. Astrophys.* **298**, 517.

Regan, P. H. (and 26 others) 1997 *Acta Phys. Pol.* B **28**, 431.

Rehm, K. E. (and 12 others) 1996 *Phys. Rev.* C **53**, 1950.

Rehm, K. E. (and 28 others) 1998 *Phys. Rev. Lett.* **80**, 676.

Rolfs, C. 1973 *Nucl. Phys* A **217**, 29.

Rolfs, C. & Barnes, C. A. 1990 *Ann. Rev. Nucl. Part. Sci.* **40**, 45.

Rolfs, C. & Rodney, W. S. 1988 *Cauldrons in the cosmos*. Chicago University Press.

Rolfs, C., Görres, J., Kettner, K. U., Lorenz-Wirzba, H., Schmalbrock, P., Trautvetter, H. P. & Verhoeven, W. 1978 *Nucl. Instrum. Meth.* **157**, 19.

Ross, J. G., Görres, J., Iliadis, C., Vouzoukas, S., Wiescher, M., Vogelaar, R. B., Utku, S., Bateman, N. & Parker, P. D. 1995 *Phys. Rev.* C **52**, 1681.

Schatz, H. (and 12 others) 1997*a* *Phys. Rep.* **294**, 168.

Schatz, H. (and 13 others) 1997*b* *Phys. Rev. Lett.* **79**, 3845.

Schmidt, S., Rolfs, C., Schulte, W. H., Trautvetter, H. P., Kavanagh, R. W., Hategan, C., Faber, S., Valnion, B. D. & Graw, G. 1995 *Nucl. Phys.* A **591**, 227.

Seuthe, S. (and 10 others) 1990 *Nucl. Phys.* A **514**, 471.

Sherrill, B., Beard, K., Benenson, W., Bloch, C., Brown, B. A., Kashy, E., Nolen, J. A., Panagiotou, A. D., van der Plicht, J. & Winfield, J. S. 1985 *Phys. Rev.* C **31**, 875.

Shore, S., Sonneborn, G., Starrfield, S., Gonzales-Riestra, R. & Polidan, S. 1994 *Astrophys. J.* **421**, 344.

Starrfield, S. 1989 *Classical novae* (ed. M. F. Bode & A. Evans). New York: Wiley.

Starrfield, S., Truran, J. W., Wiescher, M. & Sparks, W. M. 1998 *Mon. Notes R. Astr. Soc.* **296**, 502.

Stegmüller, F., Rolfs, C., Schmidt, S., Schulte, W. H., Trautvetter, H. P. & Kavanagh, R. W. 1996 *Nucl. Phys.* A **601**, 168.

Sugarbaker, E. 1995 *Nuclei in the cosmos III* (ed. M. Busso, R. Gallino & C. M. Raiteri). AIP Conference Proceedings, vol. 327. New York: American Institute of Physics.

Taam, R. M. 1985 *A. Rev. Nucl. Sci.* **35**, 1.

Taam, R. M., Woosley, S. E., Weaver, T. & Lamb, D. 1993 *Astrophys. J.* **413**, 324.

Taam, R. E., Woosley, S. E. & Lamb, D. Q. 1996 *Astrophys. J.* **459**, 271.

Taddeucci, T. N. (and 10 others) 1982 *Phys. Rev.* C **25**, 1094.

Taddeucci, T. N., Goulding, C. A., Carey, T. A., Byrd, R. C., Goodman, C. D., Gaarde, C., Larsen, J., Horen, D., Rapaport, J. & Sugarbaker E. 1987 *Nucl. Phys.* A **469**, 125.

Thielemann, F.-K., Kratz, K.-L., Pfeiffer, B., Rauscher, T., van Wormer, L. & Wiescher, M. 1994 *Nucl. Phys.* A **570**, 329c.

Timmermann, R., Becker, H. W., Rolfs, C., Schröder, U. & Trautvetter, H. P. 1989 *Nucl. Phys.* A **477**, 105.

Truran, J. W. 1982 *Essays in nuclear astrophysics* (ed. C. A. Barnes, D. D. Clayton & D. N. Schramm). Cambridge University Press.

Truran, J. W. 1990 *Physics of classical novae* (ed. A. Cassatella & R. Vietti). Berlin: Springer.

Truran, J. W. & Livio, M. 1986 *Astrophys. J* **308**, 721.

Van Wormer, L., Görres, J., Iliadis, C., Wiescher, M. & Thielemann, F.-K. 1994 *Astrophys. J.* **432**, 326.

Wagoner, R. V. 1973 *Astrophys. J.* **179**, 343.

Wallace, R. & Woosley, S. E. 1981 *Ap. J. Suppl.* **45**, 389.

Wallace, R. & Woosley, S. E. 1984 In *High energy transients in astrophysics* (ed. S. E. Woosley). AIP Conference Proceedings, vol. 115. New York: American Institute of Physics.

Wallace, R. K. & Woosley, S. E. 1985 In *Proc. of Accelerated Radioactive Beam Workshop, Parksville, Canada* (ed. L. Buchmann & J. D'Auria). Vancouver: TRIUMF.

Wanajo, S., Nomoto, K., Hashimoto, M., Kajino, T. & Kubono, S. 1997 *Nucl. Phys.* A **616**, 91c.

Weiss, A. & Truran, J. W. 1990 *Astr. Astrophys.* **238**, 178.

Wiescher, M. & Langanke, K. 1986 *Z. Phys.* A **325**, 309.

Wiescher, M., Görres, J., Thielemann, F.-K. & Ritter, H. 1986 *Astr. Astrophys.* **160**, 56.

Wiescher, M., Harms, V., Görres, J., Thielemann, F.-K. & Rybarcyk, L. 1987 *Astrophys. J.* **316**, 162.

Wiescher, M., Görres, J. & Thielemann, F.-K. 1988*a* *Astrophys. J.* **326**, 384.

Wiescher, M., Görres, J., Sherrill, B., Mohar, M., Winfield, J. S. & Brown, B. A. 1988*b* *Nucl. Phys.* A **484**, 90.

Williams, R. E. 1982 *Astrophys. J.* **261**, L77.

Wilson, J. R. & Mayle, R. W. 1988 *Phys. Rep.* **163**, 63.

Wilson, J. R. & Mayle, R. W. 1993 *Phys. Rep.* **227**, 97.

Winger, J. (and 10 others) 1993 *Phys. Rev.* C **48**, 3097.

Woosley, S. E. & Hoffman, R. D. 1992 *Astrophys. J.* **395**, 202.

Woosley, S. E. & Howard, E. M. 1990 *Astrophys. J.* **354**, L21.

Woosley, S. E. & Weaver, T. A. 1984 In *High energy transients in astrophysics* (ed. S. E. Woosley). AIP Conference Proceedings, vol. 115. New York: American Institute of Physics.

Woosley, S. E., Arnett, W. D. & Clayton, D. D. 1973 *Astrophys. J. Suppl.* **26**, 231.

Zhou, X. G., Dejbakhsh, Gagliardi, C. A., Jiang, J., Trache, L. & Tribble, R. E. 1996 *Phys. Rev.* C **53**, 982.

PHILOSOPHICAL TRANSACTIONS OF THE ROYAL SOCIETY A MATHEMATICAL, PHYSICAL & ENGINEERING SCIENCES